Pyranopterin Coordination Controls Molybdenum Electrochemistry in *Escherichia coli* Nitrate Reductase

by

Sheng Yi Wu

A thesis submitted in partial fulfillment of the requirements for the degree of

Master of Science

Department of Biochemistry
University of Alberta

Abstract

Molybdenum is an essential trace element for most species on the earth. Enzymes that contain it are called molybdoenzymes. Mononuclear molybdoenzymes play diverse roles in global geochemical cycles, bacterial metabolism, and human health. The catalytic molybdenum atom is usually incorporated into a molybdenum cofactor through a complicated biosynthetic pathway before being inserted in the enzyme. The molybdenum cofactors contain either one or two heterocyclic moieties known as pyranopterins that coordinate a single molybdenum atom with dithiolene linkages. The conventional view of the active site is that it is the immediate coordination environment of the molybdenum atom that defines catalysis. Using the *Escherichia coli* respiratory nitrate reductase (NarGHI) as a model system, I tested the hypothesis that protein coordination of the pyranopterin ring system also plays a role in defining redox chemistry and reactivity of the active site molybdenum atom. The molybdenum cofactor in the catalytic subunit NarG contains two pyranopterins coordinated by conserved residues that include a charge transfer relay (NarG-Ser719, NarG-His1163, NarG-His118, and three H_2O molecules) and two critical histidines defining the piperazine ring of pyranopterins (NarG-His1092 and NarG-His1098). NarG-Ser719 and NarG-His1163 coordinate O1 of the open pyran ring of the distal pyranopterin through H-bonds. NarG-His1184 hydrogen bonds with NarG-His1163 and three conserved H_2O molecules. NarG-His1092 links two pyranopterins via hydrogen bonding with their piperazine N-5 nitrogen atoms. The proximal piperazine N-5 nitrogen is also coordinated by NarG-His1098. The results from the charge transfer relay suggest the role of the distal pyranopterin in modulating the Mo potential and reactivity. His1092 and His1098 variants reveal the critical roles of the bridging His1092 residue and the proximal-pyranopterin-coordinating His1098 residue in controlling substrate reactivity at the Mo atom. These results support an emerging paradigm of the importance of pyranopterin coordination in defining molybdoenzyme catalysis.

Preface

Chapter 2 of the thesis has been submitted with the title *Pyranopterin Coordination Controls Molybdenum Electrochemistry in Escherichia coli Nitrate Reductase*. The framework was mostly brainstormed by Dr. Richard Rothery as a follow-up of his previous work on the pyranopterin conformational analyses in Rothery *et al.* (2012). I was responsible for the experimental planning, data collection and analyses under his direct supervision. Dr. Richard Rothery contributed significantly to the redox titration experiments and we both collected data conducting the titration experiments independently. He also provided suggestions on experimental result interpretation and the visual presentation of data analyses. I wrote the draft of the manuscript of this work. Dr. Rothery contributed to the extensive edits.

Acknowledgments

It is a great pleasure to honour the ones who have been supportive during my program years. I owe the biggest thank-you to my family. There are moments of doubts and hesitation in my life while I was in the program. I might have not been here, if there was an absence of their reassurance and encouragement.

I thank my supervisor Dr. Joel H. Weiner for taking me in as his student. I started as a summer student in 2011. I really enjoyed my internship and decided to stay in the lab for my undergraduate research project. Eventually, I became a graduate student in the lab. Joel is very open-minded and provides great freedom for me to plan and carry out my experiments independently. He is also a great role-model scientist who is always eager to learn new things.

Another big thank-you goes to our research associate, Dr. Richard Rothery. He was very knowledgeable in the field and provided detailed guidance for my thesis project. I improved my technical writing and figure making by learning from him, though I have to admit that I am still quite far away from his high standard. He and I also initialized goEdit Alberta to provide translation and editing service in technical writing. Even though it was small and we are still trying to increase our customer base, I had the opportunity to get the first-hand experience with website and business card design, and preliminary editing which is probably a rare opportunity for people at my age.

I would also like to thank my graduate student colleagues, double-Dr. Yanfei Zhang and Dr.-to-be Justin Fedor. Both of them are more senior than me and willing to share their stories and perspectives. They both offered suggestions during discussions of the project. Yanfei, in particular, shared many helpful tips with his multi-disciplinary academic background. It is also worth mentioning that both Yanfei and Justin are keeners in culinary art, and they are kind enough to share their food products. Yanfei's beef noodle soup is so far the best homemade Chinese dish I had in my seven-year Edmontonian life and Justin's liquid nitrogen ice cream is absolutely a Weiner lab specialty. Their contributions made my gut microbiome happy and therefore made me happy.

There are many more people who have been supportive to me during my program. Those people include several current and past lab members: Shannon Murphy, Michelina Kierzek, Francesca Sabastian, Glen Zhang, and Victor Cheng. I would also like to highlight some members of Department of Biochemistry who made my time in the program better: Dr. Bernard Lemire, Dr. Howard Young, and Dr. Richard Falhman who have served on my 670/671 evaluation committee and/or supervisory committee; Lucy Sun who invited to the Let's Talk Science workshops and volunteered with me for almost three years; Dr. Adrienne Wright, Dr. Jonathan Parrish, and Dr. Rachel Milner, who have been great mentors during TA sessions; and many other good friends for the company during the program. In addition, I would like to thank Dr. Xing-Zhen Chen from Department of Physiology for taking time to be my internal external committee member.

I would also like to acknowledge the International Research Training Group (IRTG) for generously providing the funding during my program and the opportunity of German exchange. I thank the Keller lab, especially Dr. Sandro Keller and PhD student Johannes Klingler, for making my stay comfortable and educational.

With all that, I would like to conclude my acknowledge section. The three year MSc program in the Department of Biochemistry at University of Alberta is an experience that I will never regret. While I will move onto the next stage of my life, I wish all the best to all my colleagues and peers.

Table of Contents

Table of Figures

List of the table

List of Abbreviations

AOR	aldehyde oxidoreductase
ATP	adenosine triphosphate
BV/BVH•	benzyl viologen/ reduced benzyl viologen
Cnx	cofactors for nitrate reductase and xanthine dehydrogenase
cPMP	cyclic pyranopterin monophosphate
DH	dehydrogenase
DmsABC	*E. coli* dimethyl sulfoxide reductase
DMSO	dimethyl sulfoxide (Me_2SO)
DMSOR	dimethyl sulfoxide reductase
EbdABC	*Aromatoleum aromaticum* ethylbenzene dehydrogenase
E. coli	*Escherichia coli*
E_m	midpoint potential
EPR	electron paramagnetic resonance
ETC	electron transport chain
FdnGHI	*E. coli* formate dehydrogenase-N
FeS	iron sulfur cluster

GTP	guanosine triphosphate
IPTG	isopropyl-1-thio-β-D-galactopyranoside
MCOS	molybdenum cofactor synthesis
MPT	molybdopterin
Mo-bisPGD	molybdo-bis(pyranopterin guanine dinucleotide)
Moco	molybdenum cofactor
Mo-enzymes	molybdoenzymes
Mo-PCD	molybdo-pyranopterin cytosine dinucleotide
Mo-PPT	molybdo-pyranopterin
MQ/MQH_2	menaquinone/menaquinol
NapA	periplasmic nitrate reductase
NarGHI	respiratory nitrate reductase
PGD	pyranopterin guanine dinucleotide
pmf	proton motive force
PMSF	phenylmethylsulfonyl fluoride
PPT	pyranopterin
Q-site	quinone binding site

SDS-PAGE	sodium docdecyl sulfate polyacrylamide gel electrophoresis
SUOX	sulfite oxidoreductase
W-enzymes	tungstoenzymes
W-bisPPT	tungsto- bispyranopterin
WT	wild-type
XDH	xanthine dehydrogenase

CHAPTER 1. Introduction

1.1 Introduction

Energy is essential for the survival of species. Many amazing adaptations in nature were solely developed to increase efficiency in obtaining food and absorbing nutrients from food. Some examples are sharp claws and teeth of carnivores for capturing and tearing preys; complex and strong digestive system of herbivores for heavy-duty digestion; and various shapes of bird beaks for catching insects and worms at different locations (1–3). This ongoing conquest of energy acquirement began at the very beginning of evolution billions of years ago at microscopic scales.

As one group of the earliest biological organisms, bacteria are an extremely diverse group of organisms living under many different conditions, some of which are considered uninhabitable to any other living thing (4, 5). Their brilliant adaptations are largely dependent on their ability to metabolize the finite amount and limited selection of substrates present in the environment. This provides an opportunity to explore bacterial bioenergetics and its role in metabolic diversity.

1.2 Bioenergetics and respiration

Bioenergetics is a biochemical field focusing on energy transformation to the cellular "currency", adenosine triphosphate (ATP), in living systems. The source of the energy can be chemical compounds, photons from the sunlight, or sometimes thermal energy. There are two common methods for cells of prokaryotes and eukaryotes to generate ATP: fermentation and respiration (6). Fermentation requires the presence of neither external electron acceptors nor the electron transport chain (ETC). It generates energy through glycolysis, in which one glucose molecule is broken down into two pyruvates with net yield of two ATP molecules and two NADH molecules. To ensure continuing glycolysis, NAD^+ is regenerated from NADH. Under anaerobic condition,

the regeneration is typically carried out by enzymes such as lactate dehydrogenase and alcohol dehydrogenase, and no ATP is produced in the process. Respiration on the other hand, requires the presence of both external electron acceptors and the ETC. The process of respiration also utilizes the glycolysis pathway; however, there are many more ATPs produced in regeneration of the electron carriers NAD^+ and FAD. Reduced NADH and $FADH_2$ are generated in process of glycolysis, Acetyl-CoA synthesis, and the Kreb cycles under aerobic conditions. In mitochondrial respiration, up to 32 ATPs are generated with initial input of one glucose through the ETC composed of Complex I (NADH:ubiquinone oxidoreductase), II (succinate:ubiquinone oxidoreductase), III (cytochrome bc_1 complex), IV (cytochome c oxidase), and V (ATP synthase) (7, 8). Complex I regenerates NAD^+ while reduces ubiquinone in the membrane to ubiquinol. Complex II oxidazes succinate (an intermediate in the Kreb cycles) to fumarate. The electrons from succinate are used to reduce FAD to $FADH_2$, from which the electrons are used to reduce ubiquinone to ubiquinol. The ubiquinol generated by Complex I and II is used to reduce cytochrome c (Fe^{3+}) to cytochrome c (Fe^{2+}) by Complex III. Complex IV reduces O_2 to H_2O with electrons from cytochrome c (Fe^{2+}). Complex I, III, and IV are capable of proton translocation by which a proton gradient is generated for ATP synthesis. The ETC allows mitochondrial respiration to be a more effective in energy production. The most common electron acceptor in biology is oxygen as in mitochondrial respiration, and the respiration is referred to as aerobic respiration. The less common electron acceptors include nitrogen, carbon, and sulfur compounds. They are more likely found in prokaryotes and allow for anaerobic respiration. Anaerobic respiration usually generates less energy than aerobic respiration, but is more efficient than fermentation.

In respiration, the pathways connecting the substrates and final electron acceptors typically involve many intermediate compounds generated in a series of chemical reactions catalyzed by multiple enzymes. The production of ATP during those reactions was explained by the chemiosmotic model proposed by Peter Mitchell in 1961(9). In his model, the electrochemical gradient of electrolytes generated by the series of chemical reactions is key to ATP synthesis. The most common electrolytes are protons and its gradient is also called the proton motive force (pmf). Proton translocation against the concentration gradient is usually coupled with the production of high-energy electrons in oxidoreduction reactions. The process requires a membrane that is impermeable to those protons to maintain the proton gradient which has a higher concentration of protons on one side and lower concentration on the other side. This accumulated potential energy from the proton gradient is the driving force for the endothermic ATP synthesis. The enzyme responsible for this process is called ATP synthase. It is a transmembrane protein that allows protons to pass through along the concentration gradient, converting the potential energy from the gradient to chemical energy of phosphodiester bonds in ATP molecules. A redox loop, also proposed by Peter Mitchell, is an example of how the proton gradient is used to create ATPs. Two coupled components, usually a dehydrogenase and a reductase, and an electron carrier are required in a loop. A dehydrogenase oxidizes its substrate and provides electron(s) for the electron carrier; a reductase uses electron(s) from the electron carrier to reduce its substrate. Protons are translocated, consumed, or generated by the dehydrogenase and the reductase during the catalysis. This normally creates a net proton difference across the membrane. A common example of redox loops is a Q cycle, which uses quinone molecules as electron carriers (10). Q stands for quinone/quinol (Q/QH_2) species, including menaquinone/menaquinol (MQ/MQH_2) and ubiquinone/ubiquinol (UQ/UQH_2). They

are able to support two-electron redox reactions with various combinations of dehydrogenases and reductases, including 15 primary dehydrogenases and 10 terminal reductases identified so far (**Figure 1.1**). Not all of listed proteins above are present in a single cell. A detailed example of *Escherichia coli* (*E. coli*) nitrate reductase A and formate dehydrogenase is illustrated in the section 1.6.1.

1.3 *E. coli* respiratory regulation

E. coli is an excellent model for studying the bacterial respiratory system and its regulation. It is a facultative anaerobic diderm bacterium that can switch its dominant metabolic pathway to adjust to the environmental oxygen level and substrate availability (10, 11). The regulation in respiration is under a strict hierarchy (12). Under aerobic condition with a sufficient amount of carbon source, the aerobic pathways are induced to use oxygen as the terminal electron acceptor for ATP synthesis, while the anaerobic pathways are repressed. When there is a lack of oxygen, the anaerobic pathways are induced. Nitrate is the preferential electron acceptor under such condition. When nitrate is not available, fumarate or dimethyl sulfoxide (DMSO) will be accepted as the next best substrate.

Such strict electron acceptor hierarchy is achieved through substantial regulation of *E. coli* gene expression. Some key regulators are the ArcB/A (aerobic respiratory control) system, FNR (fumarate nitrate reduction) protein, and Nar system. All three regulators are capable of switching the metabolism towards the anaerobic pathways under anaerobic conditions. ArcB/A and FNR are also responsible for favouring aerobic pathways over anaerobic ones through global regulations when oxygen is available (13).

ArcB/A is a two-component system with ArcB being the membrane oxygen sensor kinase/phosphatase and ArcA being the associated transcription factor in the cytosol (14–19). ArcB indirectly senses the oxygen level through the oxidation state of the quinone pool in the membrane (20, 21). ArcB is structurally composed of a 16-amino-acid transmembrane domain, a Per-Arnt-Sim (PAS) domain, and a catalytic domain. The PAS domain is a conserved feature in signal sensors that can detect changes such as light, redox states, and energy level in the cell. The PAS domain of ArcB contains key cysteine residues, Cys180 and Cys241, which can alter the function of the catalytic domain according to the quinone oxidation state. Under aerobic condition, an intermolecular disulfide bond is formed between two ArcB monomers to inhibit kinase activity, and the catalytic domain functions as a phosphatase specifically targeting phosphorylated ArcA. ArcA is not capable of interacting with DNA when dephosphorylated. Under anaerobic conditions, the two cysteines are reduced, and the catalytic domain functions as a kinase that auto-phosphorylates ArcB at conserved His292 and this phosphate group is sequentially transferred onto conserved Asp576 and His717 of ArcB (17, 18). The phosphate group on His717 is eventually transferred onto Asp54 of ArcA, and phosphorylated ArcA is capable of interacting with many *E. coli* operons globally with its helix-turn-helix motif (13, 22, 23).

Like the ArcB/A system, FNR protein is also capable of switching metabolic pathways between anaerobic and aerobic respirations (24). It is a transcription factor with an N terminus as a sensor domain and a C terminus capable of binding DNA (25). The protein binds an oxygen labile [4Fe-4S] cluster in the sensor domain under anaerobic conditions, which results in dimerization of FNR though a disulfide bond (26). The FNR dimer has enhanced ability to bind to DNA at the promoters for genes associated with anaerobic respiration (27–29). When oxygen is available,

the [4Fe-4S] cluster is converted to a [2Fe-2S] cluster through a [3Fe-4S] intermediate (26, 30–33). The [2Fe-2S]-bound FNR can no longer maintain its dimerization. As a result, the specific DNA binding is inhibited.

Unlike the previous two regulating systems, the Nar system is more specific for enhancing anaerobic respiration with the substrate nitrate. There are two homologues of the two-component Nar systems: NarX/L and NarQ/P, both of which are responsible for anaerobic respiration regulation (34). Similar to the ArcB/A system, NarX and NarQ are sensor kinases/phosphatases, and NarL and NarP are response transcription factors. NarX or NarQ senses the concentration of nitrate and nitrite (35). NarQ can bind to both substrates equally well, while NarX has a preference for nitrate. When the kinase activity of NarX is turned on by available nitrate (36), NarX autophosphorylates and transphosphorylates NarL. Phospho-NarL is capable of enhancing or repressing transcription of genes by binding to DNA. The expression of nitrate reductase is enhanced and that of fumarate reductase and DMSO reductase are repressed to ensure the nitrate metabolism is prioritized (37, 38). When there is an absence of nitrate, NarX becomes a phosphatase to dephosphorylate NarL, and the dephosphorylated NarL is no longer capable of binding to DNA. The NarQ/P system works in a similar fashion. The two parallel two-component systems are alternative to each other and ensure the nitrate/nitrite metabolism has the priority under anaerobic condition.

1.4 Molybdoenzymes and tungstoenzymes

Molybdoenzymes are an important group of enzymes catalyzing oxidoreductive reactions in respiration (39, 40). They are metalloenzymes characterized by incorporation of molybdenum, which is a rare transition metal present in the environment. They play roles in bacterial metabolic

diversity, human health, and global geochemical cycles, such as carbon, sulfur, and nitrogen cycles (41). Their presence is found in all animals and plants, and most prokaryotes.

Tungstoenzymes are analogous to molybdoenzymes (42). Current knowledge shows their presence in archaea and bacteria. Like molybdoenzymes, tungstoenzymes are also important for the metabolic diversity and global geochemical cycles (43).

1.4.1 Molybdoenzyme classification

Molybdoenzymes are classified into four families based on their cofactor coordination protein fold structure (44). They are the sulfite oxidoreductase (SUOX-fold) family, the xanthine dehydrogenase (XDH-fold) family, the aldehyde oxidoreductase (AOR-fold) family, and the dimethylsulfoxide reductase (DMSOR-fold) family. Their molybdenum cofactors and their associated functions are discussed in detail in Section 1.5.1. Most of molybdoenzymes are found in prokaryotes. The DMSOR family is the biggest family of molybdoenzymes and the most functionally diverse one. Most AOR family members are found in archaea and none from eukaryotes.

1.4.2 Molybdoenzymes in human health

Some known molybdoenzymes have a particularly important role in human health, which make the group of enzymes a research target to understand the cause of diseases and to facilitate drug discoveries (45).

Human xanthine dehydrogenase participates in purine metabolism. Deficiency or mutation can cause serious health consequences. Xanthinuria, for example, is a medical condition when purine cannot be metabolized to uric acid either due to lack of xanthine dehydrogenase (type I) or lack

of molybdenum cofactor (type II) (46). It is a disease occurring at an approximate rate of 1/69000 (47). The consequences include urinary tract calculi, acute renal failure and myositis (tissue deposition of xanthine) (48).

Human aldehyde oxidase belongs to the AOR family. The enzyme can be found in metabolic pathways of heterocycles, aldehyde, purine, and pteridine (49). It was suggested that aldehyde oxidase plays an endogenous role in the synthesis and deposition of retinoids in Hardarian glands and skin, and a role on metabolism of neurotransmitters, certain amino acid (valine, isoleucine, and leucine), and vitamins (50). It is a research target for metabolism of drugs and xenobiotics, as it is found at a high concentration in liver (51). The drugs that have been tested against aldehyde oxidase include antitumor agents (methotrexate and 6-mercaptopurine) and antidepressant (citalopram) (51–54).

Sulfite oxidase is a critical enzyme in cysteine catabolism. It converts sulfite into sulfate in the catabolic pathway. The deficiency in or mutation of sulfite oxidase can cause sulfite accumulation and toxicity (55). Molybdenum cofactor deficiency can also result in dysfunctional sulfite oxidase and the same clinical outcome. The result is severe neurodegeneration: intractable seizures, hyper- and hypotonus, mental retardation, developmental delay, and even lethality in infancy (56).

1.4.3 Molybdoenzymes in geochemical cycles

Molybdoenzymes are critical for global carbon, nitrogen, and sulfur cycles. In the nitrogen cycle, for example, molybdoenzymes participate in reactions producing different nitrogen compounds that allow nitrogen absorption and utilization by different organisms and maintain global nitrogen homeostasis between four spheres: biosphere, atmosphere, lithosphere, and hydrosphere.

Some processes involving molybdoenzymes, for instance, are nitrogen fixation, nitrogen assimilation, and nitrogen denitrification (**Figure 1.2**).

1.4.3.1 Nitrogen fixation by nitrogenase

Nitrogen is an essential element for all life found on our planet. It is an abundant element in the environment: 79% of the atmosphere volume is nitrogen. However, most organisms cannot utilize atmospheric nitrogen directly. To fulfill the demand of absorbable nitrogen, the atmospheric nitrogen is converted to nitrogen compounds and this chemical conversion is called nitrogen fixation (**Figure 1.2**). The organisms who can fix atmospheric nitrogen are called diazotrophs, and they do so through a molybdoenzyme called nitrogenase (57). It converts atmospheric nitrogen into ammonium, which is the one of nitrogen compounds absorbed by plants. Some diazotrophic bacteria and their host plants build symbiotic relationships in which the diazotrophs provide ammonium to the plants and the plants provide other nutrients to the bacteria in return. As nitrogen is typically 2% of plant weight, studies on nitrogenase became a particular interest in the field of agriculture (57). Other diazotrophic organisms are non-symbiotic and directly release ammonium into their environments and maintain the lithospheric and hydrospheric ammonium concentration for non-diazotrophic organisms.

1.4.3.2 Nitrogen assimilation by plant nitrate reductase

After inorganic nitrogen compounds are absorbed by plants, they need to be further modified for biosynthesis of biological nitrogen compounds such as amino acids and nucleotides. This is fundamental to not only plants, but also to other higher eukaryotes such as animals, as they obtain some of these nutrients directly or indirectly from plants through the food chain. This

process of converting inorganic nitrogen compounds to organic nitrogen compounds is called nitrogen assimilation.

Nitrate reduction is the first reaction in nitrogen assimilation by converting nitrate to ammonium in two steps (**Figure 1.2**). Even though both ammonium and nitrate can be absorbed by plants, ammonium can be directly used for amino acid synthesis while nitrate needs to be converted to ammonium first. The two steps are nitrate-to-nitrite conversion by nitrate reductase and nitrite-to-ammonium by nitrite reductase. Nitrate reductase is a molybdoenzyme, and it has been reported that the deficiency in molybdenum can cause deficiency in several amino acids in plants (58).

1.4.3.3 Denitrification by bacterial nitrate reductase

Similar to plant nitrate reductase, bacterial nitrate reductase also catalyzes the reaction of nitrate to nitrite. Unlike in plants, the product nitrite from bacterial nitrate reductase is further modified by a series of enzymes to molecular nitrogen (N_2), which is released to the atmosphere. The process of producing atmospheric nitrogen is called denitrification and organisms containing enzymes in the process are called denitrifiers.

Denitrifiers and diazotrophs work in the opposite direction to maintain the homeostasis between atmospheric nitrogen and nitrogen in other spheres (59). This homeostasis is interrupted in the modern history by human pollutions such as urban and agricultural runoff containing nitrate fertilizers. The excess nitrate in the water system triggers a series of natural responses called eutrophication which includes oxygen-depleted water environment caused by overgrowing algae supported by the excess nutrients, and decreased biodiversity as many aerobic species fail to compete with algae for oxygen. Because of this current crisis, denitrification became important

for wastewater treatment. Bacteria containing nitrate reductase, as denitrifiers, have been widely used in many water treatment facilities (60).

1.5 Molybdenum cofactors and tungsten cofactor

The molybdenum (tungsten) cofactor is considered one of the most important functional groups in molybdoenzymes (tungstoenzymes), if not the most important one. Studies of model molybdenum cofactors have been and still are providing information for understanding of molybdenum/tungsten cofactors (Mo-/W- cofactor). These cofactors are the signature feature of molybdo-/tungsto- enzymes (Mo-/W- enzymes) and are required for Mo/W insertion (39, 40, 61, 62). They are where redox reactions occur. The catalytic metals, molybdenum ($_{42}$Mo, period 5) and tungsten ($_{74}$W, period 6), are both d block transition metals with similar physical and chemical properties. They both have oxidation states of +6, +5, +4, +3, +2, +1, -1, and -2 and atomic radii of 39 pm. It is found that they are interchangable in some enzymes for structural assembly. Mo-/W- cofactors are energetically expensive structures, as a single molybdenum cofactor in *E. coli* requires at least five operons in its biosynthesis (63, 64). The core structure of a Mo-/W- cofactor involves a Mo or W atom coordinated by one or two pyranopterin structures. More details of their categories, structures, and functions are discussed below.

1.5.1 Categories of Mononuclear Mo-/W- cofactors

The structures of Mo-/W- cofactors vary from one Mo-/W- enzyme to another. The variation allows the cofactor to catalyze different reactions. Most Mo-/W- cofactors are mononuclear with only one metal center. A few exceptions are multinuclear cofactors, such as the iron-molybdenum cofactor ([$MoFe_7S_9$] cluster) from nitrogenase (65, 66). Only mononuclear

Mo-/W- cofactors will be discussed herein. A Mo-/W- cofactor is so important for the enzyme that the classification of Mo-/W- enzymes is based on the type of protein fold coordinating the Mo-/W- cofactors. The complexity of the cofactor is positively correlated to the level of substrate variation (44, 63, 67). The four categories of Mo-/W- enzymes in the order of increasing cofactor complexity are sulfite oxidoreductase (SUOX-fold) family, xanthine dehydrogenase (XDH-fold) family, aldehyde oxidoreductase (AOR-fold) family, and dimethylsulfoxide reductase (DMSOR-fold) family. The four general types of Mo-/W- cofactors and their corresponding Mo-/W-enzymes are illustrated in **Figure 1.3** and discussed in details below.

1.5.1.1 Simplest molybdo-pyranopterin cofactor (Mo-PPT)

The simplest form of a Mo-/W- cofactor is the molybdo-pyranopterin structure (Mo-PPT) with mononuclear molybdenum coordinated by a single pyranopterin. With current structure information, this type of cofactor is present in all eukaryotic molybdoenzymes, all SUOX family members, and some bacterial XDH family members. SUOX family enzymes are present in bacteria, plants, and animals. Many of them are important for sulfur metabolism in living systems and deficiency or mutations can sometimes lead to severe consequences including lethality. Examples are sulfite oxidase from *Gallus gallus* and *Arabidopsis thaliana* and sulfite dehydrogenase from *Starkeya novella*. Assimilatory nitrate reductase also belongs to this family. In addition, there are another two enzymes in the SUOX family with unknown functions: YedY and YuiH (68). They are under current investigation to determine their roles. The SUOX family functional distribution is concluded in **Figure 1.4**. The simple molybdo-pyranopterin cofactors are also found in some bacterial XDH proteins such as *Rhodobacter capsulatus* xanthine dehydrogenase.

1.5.1.2 Molybdo-pyranopterin cytosine dinucleotide (Mo-PCD)

The molybdo-pyranopterin cytosine dinucleotide has a structural addition to the simplest molybdo-pyranopterin cofactors — cytosine dinucleotide. The cytosine dinucleotide is covalently linked to the pyranopterin through a phosphoester bond. This type of cofactor is incorporated in most bacterial members of the XDH family. Some examples are *Desulfovibrio gigas* aldehyde dehydrogenase, *Pseudomonas putida* isoquinoline oxidoreductase, and *Thauera aromatica* 4-hydroxybenzoyl-CoA reductase (69). About half of the XDH family catalyzes purine metabolism, and the rest catalyzes reactions on isoquinoline, niacin (B3γ 4-hydroxybenzoyl-CoA), aldehyde, carbon monoxide, and other substrates (**Figure 1.5**). A modified Mo-PCD has been found in carbon monoxide oxidoreductase from *Oligotropha carboxidovorans* (70). This unique dinuclear heterometal cofactor contains a Cu atom in addition to the Mo atom and is denoted as (CuSMo(O=)OH) (71).

1.5.1.3 Tungsto-bispyranopterin (W-bisPPT)

The third complex level of Mo-/W- cofactor is featured by two pyranopterins forming two dithiolene linkages instead of one pyranopterin in the previous two levels. It is found in AOR family members, many of whom are in archaeal proteins. Examples are aldehyde:ferrodoxin oxidoreductase and formaldehyde oxidoreductase in thermophilic *pyrococcus furiosus* (72–74). The cofactor is quite weak on functional diversity despite its complexity: the functions of the AOR family members are limited to aldehyde and formaldehyde catalysis as shown in **Figure 1.6**.

1.5.1.4 Molybdo-bis (pyranopterin guanine dinucleotide) (Mo-bisPGD)

This is the most structurally complex and functionally diverse category of Mo-/W- cofactors. In addition to the structure of the central metal coordinated by two pyranopterins as in W-bisPPT, two guanine nucleotides are covalently linked to the pyranopterins. This type of cofactor is found in the DMSOR family of Mo-/W- enzymes and utilizes diverse substrates as shown in **Figure 1.7**. The cofactor is present in the following enzymes: formate dehydrogenases, S- and O-oxidoreductase, nitrate/selenate/percholorate reductases, sulfur anion reductases, formylmethanofuran dehydrogenases, arsenite oxidases, and many other enzymes with known or unknown functions (44). The metabolic diversity of DMSOR family is suggested as a result of Mo electron potential variation, such as $E_{m,pH8}$ = -420 mV for *E. coli* formate dehydrogenase, and $E_{m,pH8}$ = +420 mV for *E. coli* nitrate reductase. The Mo electron potential is determined by its coordinating environment. The impact of its surrounding dithiolene linkage, protein ligand(s), and general protein environment has been investigated for decades.

1.5.2 Pyranopterin (PPT)

A pyranopterin refers to a cofactor component coordinating a metal ion through sulfur atoms. It is a conserved feature of molybdenum or tungsten cofactor. Most pyranopterins are in tricyclic form consisted of a pyran, a pyrimidine, and a piperazine ring. In bis-pyranopterin cofactors, the two pyranopterins are named according to their distance to the juxtapositional iron sulfur cluster present in almost all DMSOR family enzymes: the pyranopterin positioned closer to the iron sulfur cluster is named the proximal pyranopterin, and the farther one is named the distal pyranopterin (75, 76). A bicyclic pyranopterin with open pyran ring has been observed in *E. coli* NarGHI and ethylbenzene dehydrogenase (77, 78). The number of pyranopterins in a cofactor is

important for cofactor classification: the simplest Mo-PPT and Mo-PCT contain one pyranopterin, and more complex W-bisPPT and Mo-bisPGD contain two pyranopterins.

1.5.2.1 Pyranopterin conformational analysis

The three dimensional conformation of a pyranopterin is influenced by redox states of the ring structure and the interaction of the pyranopterin with the surrounding protein environment. Pyranopterins are highly enriched with double bonds, which is common in electron-carrying prosthetic groups. The carbon atoms in a double bond can adopt sp^2 hybridization which allows electron delocalisation and a more planar pyranopterin conformation. A change in the pyranopterin redox states alters the electron distribution in the pyranopterin ring structures, and therefore, the conformation of the pyranopterin. Interactions such as hydrogen bonding, electrostatic interaction, and hydrophobic interaction also influence the conformation of a pyranopterin.

In Rothery *et al.* 2012, it was determined that the conformations of distal and proximal pyranopterins are different: the proximal pyranopterin adopts a more distorted structure in comparison to the distal pyranopterin (76). The distortion is most significant at pyrazine and pyran ring positions. The analyses indicated the oxidation state varies between the two pyranopterins. The more distorted proximal pyranopterin is in the more reduced tetrahydro form and the distal pyranopterin is in the more oxidized 10-10a dihydro form. The structural assignment suggests this pattern is systemic in all bis-pyranopterin cofactors of DMSOR family members. The pyranopterin of XDH family members adopts the conformation of DMSOR proximal pyranopterin, and the pyranopterin of SUOX family members adopts the conformation of DMSOR distal pyranopterin as shown in **Figure 1.8**. Both XDH pyranopterins and proximal DMSO pyranopterins are located between the Mo and the nearest FeS cluster; both SUOX

pyranopterins and distal DMSO pyranopterins are located on the other side of the Mo, away from the closest FeS cluster in the electron transfer system (76). This suggests the tetrahydro form of the pyranopterin may serve a role in electron flow between FeS cluster and Mo and the dihydro form may serve a different role. This is the first study that suggests a functional division between the two pyranopterin in bis-pyranopterin cofactors.

1.5.3 Biosynthesis of Mo-/W- cofactors

Mo-/W- cofactors in general are complex structures requiring many proteins to be properly synthesized and incorporated into an apoenzyme. The biosynthesis of a molybdenum cofactors is divided into four steps based on intermediates precursor Z, molybdo-pterin (MPT), and adenylated MPT; and the product Moco (62, 63, 67). The synthetic pathways are well conserved for molybdenum cofactors. There are six proteins identified for such purpose in fungi, plants, and humans (79–83). They are homologues of their prokaryotic counterparts. The prokaryotic proteins can functionally substitute for the eukaryotic proteins. Genes and proteins for Moco synthesis use the nomenclature cnx (cofactor for nitrate reductase and xanthine dehydrogenase) in plants and MCOS (molybdenum cofactor synthesis) in humans. The biosynthetic process is summarized in **Figure 1.9** and discussed below.

1.5.3.1 Circularization of GTP to form cPMP

The first step is to convert 5'- GTP (5'- Guanosine triphosphate) to cPMP (cyclic pyranopterin monophosphate) (84). The intermediate cPMP is the most stable species in the pathway of Moco biosynthesis (85). Its structure was solved by H-NMR, showing a fully reduced tricyclic tetrahydro structure (86, 87). The cPMP is formed by radical rearrangement of GTP, supported by the observation in the H-NMR experiments that all the C atoms from labelled GTP become

part of cPMP (88). The intermediate cPMP is still sulfur-free. There are two proteins responsible for the conversion of GTP to cPMP:

(1) Radical S-adenosylmethionine (SAM)-dependent enzyme

The name for the enzyme is Cnx2 in plants, MOCS1A in humans, and MoaA in bacteria *E. coli* and *S. aureus* (89). The enzyme catalyzes the rearrangement of the GTP in which the one-ring deoxyribose group is fused with the two-ring guanine nitrogen base to form a tricyclic structure (90). This free-radical reaction is catalyzed by the radical SAM. FeS clusters found in radical SAM-dependent enzyme are important in generating the radical SAM (89). The entire reaction mechanism is well defined in MoaA (84, 91). The mechanism for Cnx2 and MOCS1A is speculated to be similar, as they can be used to substitute MoaA (82, 92). The N-terminal [4Fe-4S] cluster of MoaA binds SAM, which leads to subsequent reductive cleavage of SAM, resulting in a 5'-deoxyadenosyl radical. The radical can initiate further reaction to transform the GTP into a tricyclic structure.

(2) Functionally unknown protein

The identified members of the protein are Cnx3 in plants, MOCS1B in humans, and MoaC in bacteria. The function of the protein is not identified yet. MoaC, for instance, has no sequence or structural similarity to any functionally identified protein group (93). One speculation is that the protein is involved in pyrophosphate release during molecular rearrangement (63). There are other proposals for its involvement in the catalysis, such as anionic charge stabilization (93).

1.5.3.2 Formation of dithiolene group to form MPT

The second step involves MPT (molybdopterin) synthesis, where sulfur is added to the cPMP. The enzyme that catalyzes this step is called MPT synthase. It is a heterotetrameric protein

complex consisting of two small subunits (plant Cnx7, *E. coli* MoaD, or human MOCS2B) and two large subunits (plant Cnx6, *E. coli* MoaE, or human MOCS2A). The sulfur atom for transfer is bound to the C-terminus of a small subunit as a thiocarboxylate group. The C-terminal region is well conserved, with a conserved double glycine feature where thiocarboxylation occurs (94, 95).

The mechanism of MPT synthase is characterized in *E. coli* MPT synthase (67). *E. coli* MPT synthase is an elongated complex containing two active sites, each formed by the C-terminus of a small subunit deeply inserted into a large subunit (96). The two separate active sites also suggest that the two sulfur groups are not simultaneously transferred, as verified by the observation of a monosulfurated intermediate (97). The sulfuration site is on C2' of the cPMP molecule. There is one question remaining: whether the intermediate, the cPMP molecule with a single thiolene, is transferred to the other active site through the complex or dissociates from the complex first. There is little direct knowledge on the catalytic mechanism of MPT synthase from other organisms; however, it has been noticed that the exchange of large subunits between species allow the complex to function (94). It is reasonable to conclude that the catalytic mechanism is the same in MPT synthases from different species.

Another enzyme worth mentioning is the MPT-synthase sulfurase (plant Cnx5, *E. coli* MoaB, or Human MOCS3). This enzyme resulfurates the small subunit C terminal double-glycine after a cycle of sulfur transfer catalysis. The protein contains two domains. The N-terminal domain is an adenylating domain and the C-terminal domain is a rhodanese-like domain (RLD) where sulfur bound to a conserved Cys forms persulfide (98, 99). The two domains allow the protein to be multifunctional: after sulfur transfer by the RLD domain, the resulfurated MPT synthase small

subunit is activated through adenylation by the adenylating domain of MPT-synthase resulfurase (100).

1.5.3.3 Formation of MPT-AMP

The formation of intermediate MPT-AMP is characterized in plant Cnx1 and verified in *E. coli* MogA (67). Cnx 1 contains a G-domain for adenylation and an E-domain for Mo-insertion. The two reactions are catalyzed by two separate enzymes in *E.coli*: MogA for adenylation and MoeA for Mo-insertion. The adenylation reaction catalyzed by the Cnx1 G-domain is Mg^{2+} and ATP dependent. The high-energy MPT-AMP intermediate energetically favours the subsequent Mo insertion, as the transfer of molybdate from the molybdate uptake system to MPT pathway is a non-spontaneous process.

1.5.3.4 Mo insertion

The enzyme responsible for Mo ligation to MPT is Mo-insertase (plant Cnx1, *E. coli* MogA/MoeA, and human Gephyrin). It has been shown that a defective mutation in the Mo-insertase Cnx1 can be rescued by a high level of molybdate (1-10mM) which does not occur physiologically (101). Mo-insertion is carried out by Cnx1 E-domain in plants. The hydrolysis of MPT-AMP is a Mg^{2+} and molybdate dependant reaction (102, 103). The end product is a MPT in which the Mo bonds with two oxo ligands and one deprotonated hydroxyl group (102).

The presence of Cu was observed in a Cnx1G crystal structure (40, 86). The metal binds to MPT dithiolate sulfur in a tetragonal coordination. This is an indication of metal replacement event where Cu acts as the leaving group and Mo comes for replacement. It is speculated that Cu protects MPT dithiolate from oxidation.

1.6 NarGHI

1.6.1 Overview

E. coli nitrate reductase A (NarGHI) is a molybdoenzyme with a Mo-bisPGD cofactor. As an important member of *E. coli* respiratory proteins, it can couple with dehydrogenases to complete a redox loop for anaerobic respiration (104). One example involves the redox loop formed by *E. coli* nitrate reductase and formate dehydrogenase (FdnGHI) as illustrate in **Figure 1.10**. The periplasm-facing FdnGHI reduces menaquinone to menaquinol in the membrane pool, and the cytoplasm-facing NarGHI oxidizes menaquinol and reduces nitrate to nitrite (105). The cycles of generation and consumption of menaquinol allows the loop to continue. The two proteins are oriented in opposite directions to allow the two scalar reactions to create a vectorial reaction where a unidirectional proton gradient is generated. The detailed proton translocation is described in **Figure 1.10** and chemical reactions below. For each cycle, seven-proton difference across membrane is created: two protons are consumed in cytoplasmic nitrate reduction by NarGHI; one proton is released into the periplasm by FdnGHI; two protons are picked up by menaquinone from the cytoplasmic side and released into the periplasmic side after menaquinol oxidation by NarGHI (78). The reactions are illustrated below:

NarGHI: $NO_3^- + MQH_2 + 2H^+$ (cytoplasm) → $NO_2^- + H_2O + MQ + 2H^+$ (periplasm)

$\Delta H^+ = 4$

FdnGHI: $HCOO^- + MQ + 2H^+$ (cytoplasm) → $CO_2 + MQH_2 + H^+$ (periplasm)

$\Delta H^+ = 3$

Net reaction: $NO_3^- + HCOO^- + 4H^+$ (cytoplasm) $\rightarrow NO_2^- + CO_2 + H_2O + 3H^+$ (periplasm)

$\Delta H^+ = 7$

To further explore the mechanism of NarGHI, the structure of this important enzyme was determined as described in Bertero *et.al*. *Nature Structural & Molecular Biology* (2003) (78). NarGHI is a cytoplasmic membrane-bound heterotrimeric protein facing the cytoplasm and is found in a functional unit of homodimers. The three subunits are named NarG (catalytic subunit), NarH (electron transfer subunit), and NarI (membrane anchor subunit). The complex has a dimension of 90 X 128 X 70 Å and a size of 223,921 Da. It contains 1983 amino acid residues and 8 prosthetic groups.

1.6.2 The *nar* operon

The typical *nar* operon is in a cluster of *nar*XL-*nar*K-*nar*GHJI. *nar*XL encodes for NarX/L two-component regulatory complex, which has positive impact on expression of Nar proteins when there is a lack of oxygen and presence of nitrate (106). *nar*K encodes for nitrate and/or nitrite transporter and usually presents in one or two copies of the genes (107). *nar*GHJI encodes for the membrane-bound nitrate reductase NarGHI. NarJ is not a part of an active NarGHI, but a very critical chaperone for NarGHI (108). During the enzyme assembly process, NarJ binds NarG of the apoenzyme NarGH to keep it at a conformation for Moco insertion (109). After Moco incorporation, NarJ dissociates from the complex before NarGH attaches to NarI on the membrane.

1.6.3 NarG

NarG is the catalytic subunit which contains 1246 amino acid residues and two prothetic groups: the molybdenum cofactor and [4Fe-4S] cluster FS0 (78). The protein component of NarG

structurally consists of four conserved α-β domains denoted as Domains I to IV. The domains are illustrated in Fig. 1.11 and some of their functions are highlighted in detail below.

Domain I consists of 2 mixed β sheets, 3 α helices and a structured N-terminal tail (78). One of its roles is to coordinate FS0 though His50, Cys54, Cys58, and Cys93. The combination of one histidine and three cysteine as FeS ligands is relatively uncommon and has only been previously observed in the [Ni-Fe] hydrogenase from *Desulfovibrio gigas* and the Fe-only hydrogenase from *Clostridium pasteurianum* (110). Based on the calculation of edge-to-edge distance, FS0 is 7 Å and 11 Å away from Mo-bisPGD and FS1, respectively. The protein environment surrounding the FS0 contains many aromatic residues to stabilize its redox potential. The N-terminal tail extended from Domain I serves as a regulatory/accessory protein binding site and is important for enzyme assembly. It is where NarH interacts with NarG to form the NarGH complex. In addition, the nitrate reductase chaperone NarJ binds at the N terminus to ensure proper incorporation of Moco and delivery of complex NarGH to the membrane domain NarI (108).

Domain II and III are formed by mixed α-β structure and important in coordinating Mo-bisPGD. Domain II interacts with the proximal pyranopterin of the Mo-bisPGD, and Domain III links to the distal pyranopterin (78). The two pyranopterins and their interacting partners will be explained in detail in Section 1.6.6. It is also evident that the residues at the Mo active site may play a role in enzyme catalytic mechanism and details are also included in Section 1.6.6.

1.6.4 NarH

The electron transfer subunit NarH contains 512 residues and four iron-sulfur clusters that each is capable of holding one electron at a time. The subunit belongs to the superfamily of bacterial

oxidoreductase electron transfer subunits. This subunit is important in transferring the electron from NarI to NarG. There are two domains in NarH, and each of them holds one high-potential FeS cluster and one low-potential FS cluster (78). The two high-potential FeS clusters are FS1 and FS4 with midpoint potentials of 130 mV and 180 mV, respectively; the two low-potential FeS clusters are FS2 and FS3 with midpoint potentials of -420 mV and -55 mV, respectively. The underlying cause for the variation in the midpoint potential of iron sulfur clusters is not clearly identified yet. Some speculated causes are the degree of hydrophobic interactions, protein folds, surrounding residues, or solvent interactions. With electrons flowing from FS1 to FS4 in sequence as illustrated in **Figure 1.11**, it is important to recognize that the midpoint potentials of FeS clusters are not exactly in an increasing order. However, the overall potential difference between FS1 and FS4 (50 mV) is significant enough to drive the electron flow.

The FeS clusters are ubiquitous structures found in electron transfer enzymes and studies of their function, structure, and biosynthesis have been conducted to obtain a comprehensive understanding of them (111). To obtain a more detailed understanding of the FeS clusters involved in NarGHI, we need to examine their structures. With the exception of FS4 being a [3Fe-4S] cluster, all other FeS clusters are [4Fe-4S]. The [4Fe-4S] clusters have alternating Fe and S in a cubane structure in which each iron coordinates with three sulfur atoms (112). The [3Fe-4S] cluster has one fewer iron, with three sulfur atoms each coordinating two irons and the fourth sulfur coordinating three irons. The structure of the cluster is very different from that of the [4Fe-4S] cluster (113). In both [4Fe-4S] and [3Fe-4S] clusters, each iron is coordinated by Cys residues of NarH. The mutation of Cys can cause detrimental effects on electron transfer as previously indicated in other iron-sulfur enzymes such as fumarate reductase and DMSO reductase (114, 115).

1.6.5 NarI

The subunit NarI contains 225 amino acids and two low-spin heme groups, the proximal heme (Heme b_P) and the distal heme (Heme b_D). The proximal heme is closer to the NarGH than the distal heme. The detailed structure is shown in **Figure 1.13**. The protein component of NarI contains five transmembrane helices, denoted as TM I to V, and two horizontal helices between TM IV and TM V, denoted as helices 2 and 3_{10} (78). The transmembrane helices are 30° tilted from the normal of the membrane bilayer. The C terminus of the subunit interacts with NarGH complex to assemble and stabilize the heterotrimeric structure, NarGHI.

The heme groups in NarI are important redox cofactors and have been studied to a great extent. Heme b_D is where the menaquinol oxidation occurs, which is the rate-limiting step of the entire NarGHI catalysis. The two electrons from the quinol are passed sequentially through hemes towards the Moco. The equations of menaquinol oxidation/heme reduction are below.

Q site: $MQH_2 \rightarrow MQ + 2H^+ + 2e^-$

Heme b_D: oxidized Heme $b_D + e^- \rightarrow$ reduced Heme b_D

Overall: 2 oxidized Heme $b_D + MQH_2 \rightarrow 2$ reduced Heme $b_D + MQ + 2H^+$

(Note: There is only one Heme b_D in the structure. The reduced Heme b_D passes its electron to Heme b_P before accepting the second electron from menaquinol. Thus, Heme b_D is reduced twice by the electrons from one menaquinol molecule)

The reaction described is greatly facilitated by the protein environment in NarI. Several conserved residues at the Q site have been found to be critical for menaquinol binding and oxidation. Lys 86, in particular, shows great flexibility between different side chain orientations

in different crystal structures, and is speculated as a swing arm to modulate the protonation state of heme b_D for the reaction (116).

1.6.6 NarGHI Molybdo-bis (pyranopterin guanine dinucleotide) (Mo-bisPGD)

With NarGHI belonging to the DMSOR family, its cofactor is in the group of Mo-bisPGD cofactors. This is where the nitrate reduction occurs. The Mo atom of this cofactor can reach all the biological accessible oxidation states: +4, +5, and +6. Because all the hemes and FeS clusters can only hold one electron at a time, the two electrons from menaquinol are passed through the prosthetic groups one by one. The Mo-bisPGD can hold the first electron and wait for the other one. When both electrons are received, the cofactor carries out two-electron reduction to convert nitrate to nitrite. The net reaction is described in the following equation:

$$NO_3^- + 2e^- + 2H^+ \rightarrow \quad NO_2^- + H_2O$$

Molybdenum coordination plays an essential role in the nitrate reduction catalytic mechanism. The Mo atom can have six coordination partners, of which four are dithiolene sulfurs from the MPTs. The last two coordinations are filled with a bidentate coordination of carboxyl oxygens of residue NarG-Asp222, or an oxo group with or without a monodentate coordination of Asp 222 carboxyl group (**Figure 1.14**) (78). An Asp or Glu residue at the position of molybdenum active site is highly conserved and the carboxylate group from either residue appears to be critical (117). Asp222 adds additional chelation through monodentate coordination from one oxo group of the Asp side chain or bidentate coordination from both oxo groups. The alteration between the two forms is speculated to have a role in change of Mo oxidation state between +4 and +6. The monodentate and bidentate coordinations were seen in two crystal structures solved

independently (1Q16 and 1R27). The oxidation state of Mo in the sample prepared for X-ray crystallography was presumed at +6 due to the presence of atmospheric oxygen during the experiment; however, it is possible the Mo atom was reduced by the high-energy X-ray laser. The alteration between Asp222 monodentate and bidentate coordinations in structures may represent different stages of catalysis.

The Mo-bisPGD is coordinated by the conserved residues from NarG which includes His1098, His1163, His1092, Val578, Asp222, and Tyr220. Among those residues, some residues such as Asp222, His546, and Asn1217 may be involved in Mo catalysis. The Asp222, as mentioned earlier, can modulate the Mo oxidation states. It can be coordinated by His546 and His546 is coordinated by Asn1217 (78, 118). A mechanism was proposed in our lab in which Asp222 maintains a bidentate coordination to the Mo(IV) until the nucleophilic attack from NO_3^- oxygen (**Figure 1.14**). Then, the Asp switches to a monodentate coordination and the other oxygen of the carboxyl group is stabilized by the His546. At this moment, Mo(IV) is coordinated by one oxygen of NO_3^- and one oxygen from Asp222. Further rearrangement of the molecular complex occurs when two electrons from the molybdenum leave for nitrate reduction. A nitrite is formed and leaves behind an oxo group coordinating Mo(VI). Upon receiving another two electrons from the membrane menaquinol, the oxo group is released as a H_2O molecule, and Asp222 re-establish its bidentate coordination to the Mo(IV).

1.7 Thesis objectives

The role of pyranopterins has been perceived as the structural anchor for the Mo. In other words, pyranopterins are chemically innocent. The overall reduction potential of Mo is controlled by its

dithiolene bonds with Mo, protein ligand(s) such as Ser and Asp, and overall protein environment. The rest of the cofactor is entirely for structural support.

Based on research in the lab and studies with model compounds, we proposed that the pyranopterins are more than a structural support (76, 119–121). First, the complexity and energy consumption of pyranopterin synthesis suggested likelihood that pyranopterins are more important than an anchor, since the structural support can be provided by a much simpler structure such as Cys residues. Second, conformational analyses indicated that two pyranopterins in bispyranopterin cofactors systematically adopt different conformations. The conformational difference suggests potentially different roles for the two pyranopterins in addition to their supporting role.

Based on available structural information and previous conservation analysis, we propose that pyranopterins are involved in modulation of Mo electron chemistry. To be more specific, the hypothesis involves the following.

(1) The proximal pyranopterin is acting as an electron conduit to conduct electrons from FS0 towards Mo;
(2) The distal pyranopterin plays a role in fine-tuning electron potential of Mo through conserved charge transfer relay (NarG-His1163, His1184, and three water molecules).

We conducted our experiments by characterizing the electron potential and activity of variants of important conserved residues involved in coordinating the pyranopterins. They are divided into two groups:

(1) His1163, His1184 and Ser719 coordinating the distal pyranopterin;

(2) His1092 bridging the proximal and distal pyranopterins, and His1098 coordinating the proximal pyranopterin.

1.8 Figures

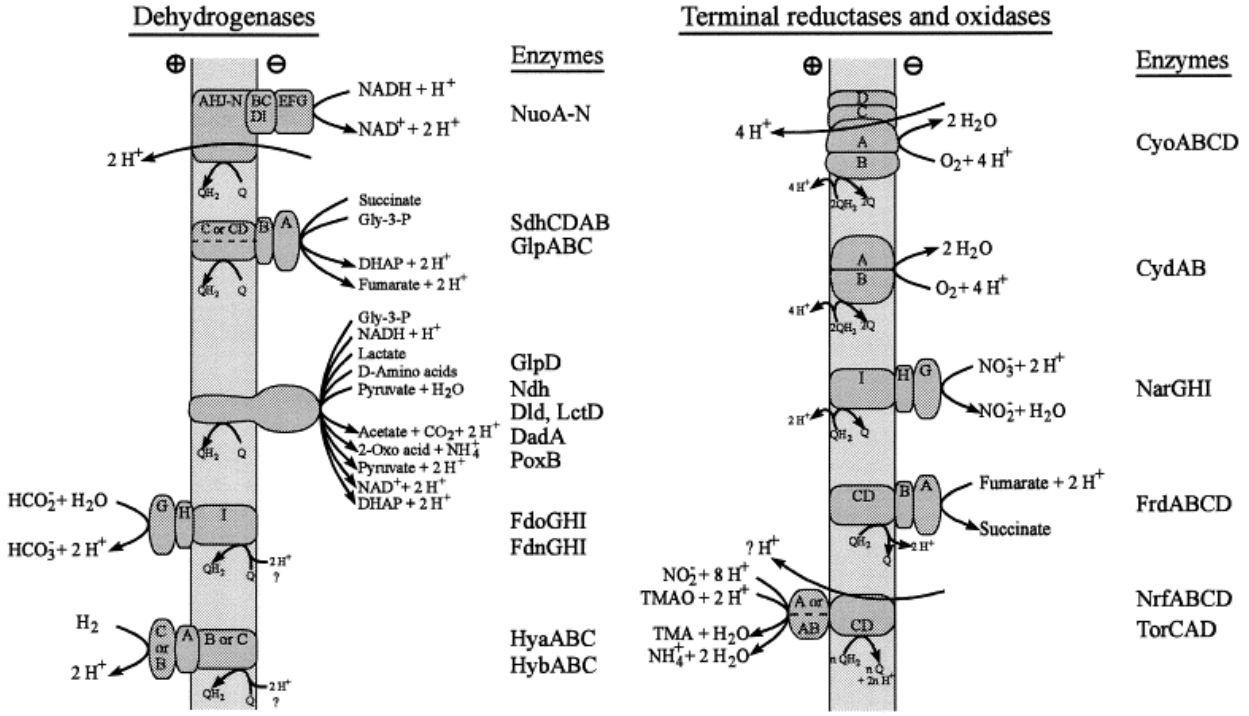

Figure 1.1. Dehydrogenases and reductases

The figure illustrates metabolic dehydrogenases on the left side and terminal reductases on the right side. All the above enzymes are aerobic or anaerobic respiratory enzymes in *E. coli*. The combination of a dehydrogenase and a reductase forms a redox loop via an electron carrier quinol molecule from the membrane Q-pool. The redox loop is usually coupled with proton gradient generation. The dehydrogenases are NADH dehydrogenase I (NuoA-N), succinate dehydrogenase (SdhCDAB), glycerol-3-phosphate dehydrogenase/DH_O (GlpABC), glycerol-3-phophate dehydrogenase/DH_N (GlpD), NADH dehydrogenase II (Ndh), D-lactate dehydrogenase (Dld), L-lactate dehydrogenase (LetD), D-amino acid dehydrogenase (DadA), pyruvae oxidase (PoxB), formate dehydrogenase/DH_O (FdoGHI) formate dehydrogenase/DH_N (FdnGHI), hydrogenase 1 (HyaABC), and hydrogenase 2 (HybABC). The terminal reductases are quinol oxidase bo_3 (CyoABCD), quinol oxidase bd (CydAB), nitrate reductase A (NarGHI), fumarate reductase (FrdABCD), nitrite reductase (NrfABCD), and TMAO reductase (TorCAD). This figure is adapted from Unden,G., and Bongaerts, J. (1997) (10).

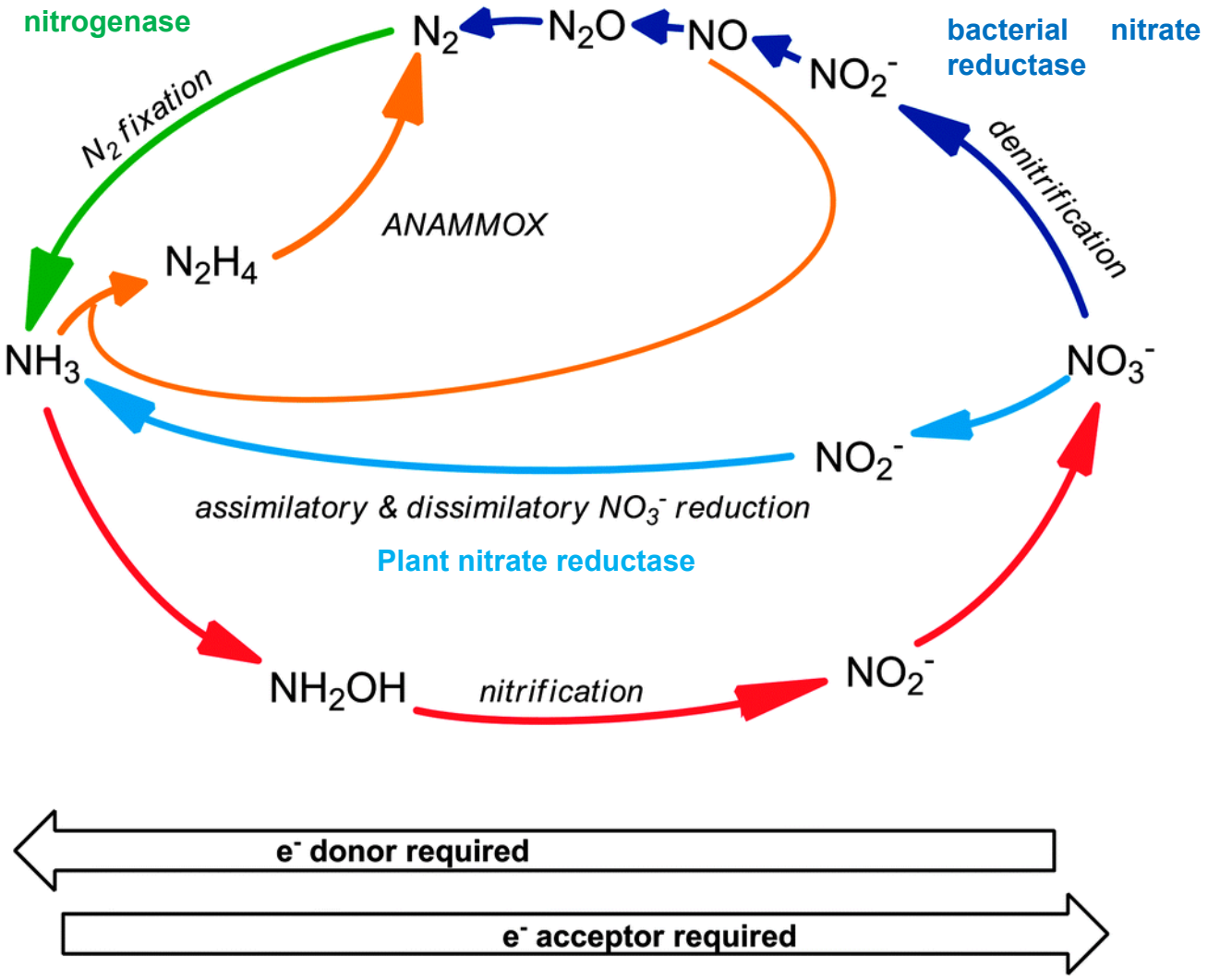

Figure 1.2. Global nitrogen homeostasis is maintained by the nitrogen cycle.

The nitrogen cycle is completed by many processes including nitrification, nitrogen assimilation, nitrogen fixation, and denitrification. Many molybdoenzymes participate in reactions above and some are highlighted: nitrogenase in green, plant nitrate reductase in light blue, and bacterial nitrate reductase in dark blue. The figure is modified from Sparacino-Watkins *et al*. (2014) (122).

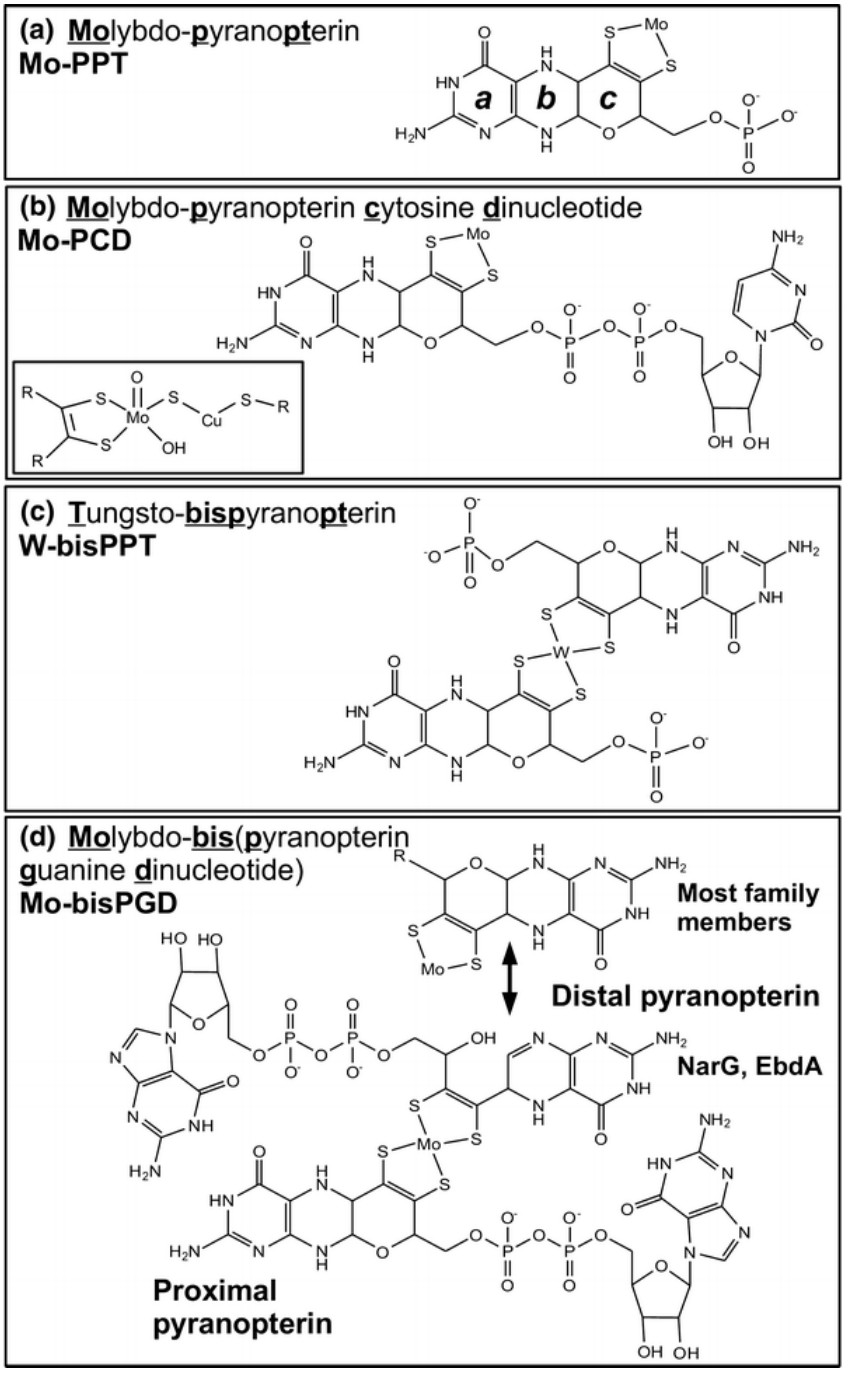

Figure 1.3. Molybdenum cofactor classification

The molybdenum/tungsten cofactor is categorized into four levels based on their component and complexity. (a) Mo-PPT contains one pyranopterin coordinating the molybdenum; (b) Mo-PCD contains the basic structure of a Mo-PPT with an additional nucleotide group (cytosine); the inset illustrates a special structure from carbon monoxide oxidoreductase; (c) W-bisPPT contains two pyranopterins coordinating a tungsten atom; (d) Mo-bisPGD contains two pyranopterins each linked to a GDP group. The figure is adapted from Rothery *et al*. (2015) (44).

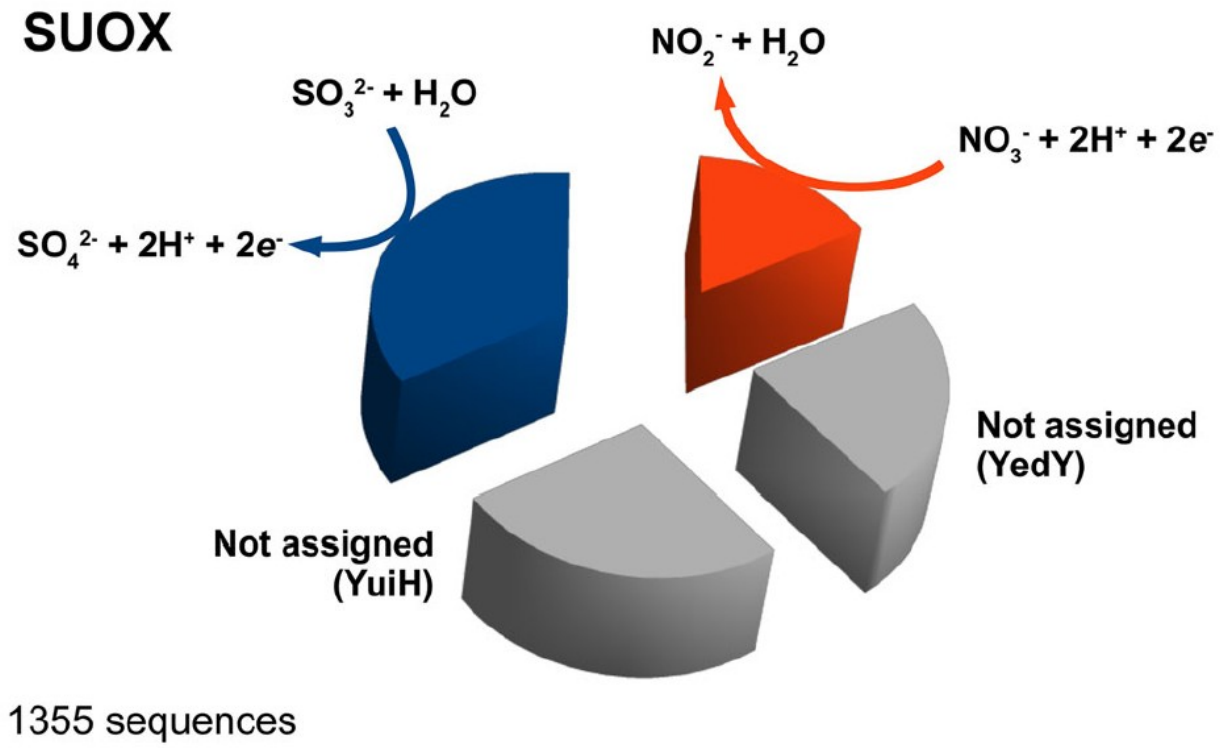

Figure 1.4. SUOX family functional distribution

The distribution of SUOX family molybdoenzymes are illustrated in the diagram. The blue portion represents a significant proportion of SUOX family members that catalyzes sulfate reduction to sulfite. The orange part represents the portion of members catalyzing nitrite oxidation to nitrate. The grey portions are YuiH and YedY with unknown function(s). The figure is adapted from Rothery *et al*. (2015) (44).

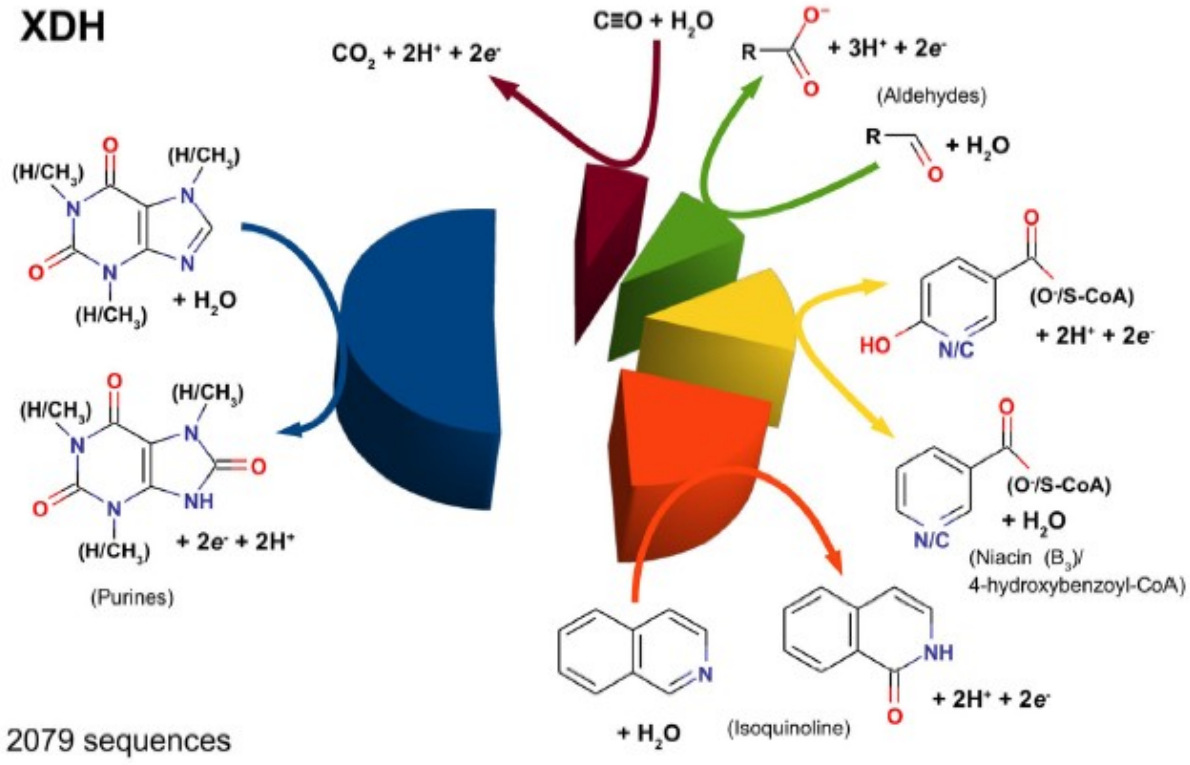

Figure 1.5. XDH family functional distribution

The figure illustrates the functional distribution of the XDH family. The blue part represents about half of the XDH family members that catalyzing purine metabolism. The dark red part is a small percentage of XDH family members catalyzing carbon monoxide oxidation to carbon dioxide. The green part, yellow part, and orange part represent the XDH family members catalyzing aldehyde oxidation, niacin oxidation, and isoquinoline oxidation, respectively. The figure is adapted from Rothery *et al*. (2015) (44).

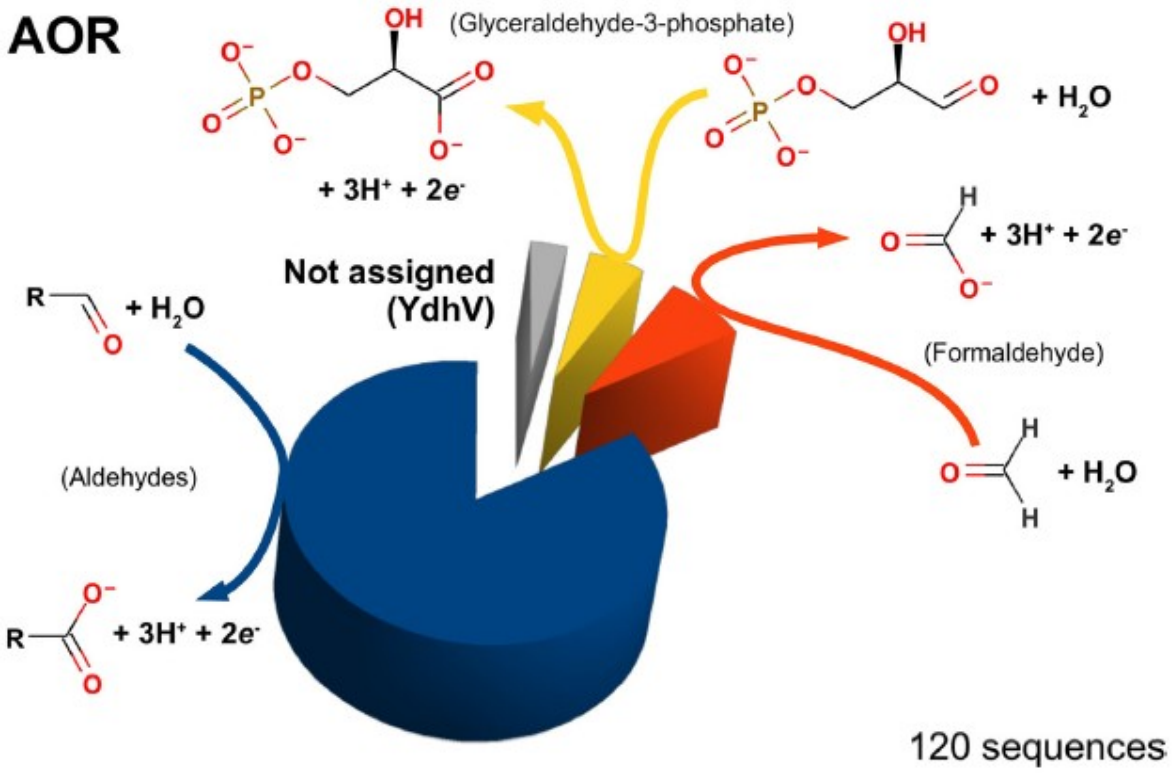

Figure 1.6. AOR family functional distribution

The figure illustrates the functional distribution of AOR family members of molybdoenzymes. Most AOR family members are aldehyde oxidizing represented by blue. The grey, yellow and orange represent YdhV with unknown function, Glyceraldehyde-3-phosphate oxidizing enzymes, and formaldehyde oxidizing enzymes, respectively. The figure is adapted from Rothery *et al*. (2014) (44).

.

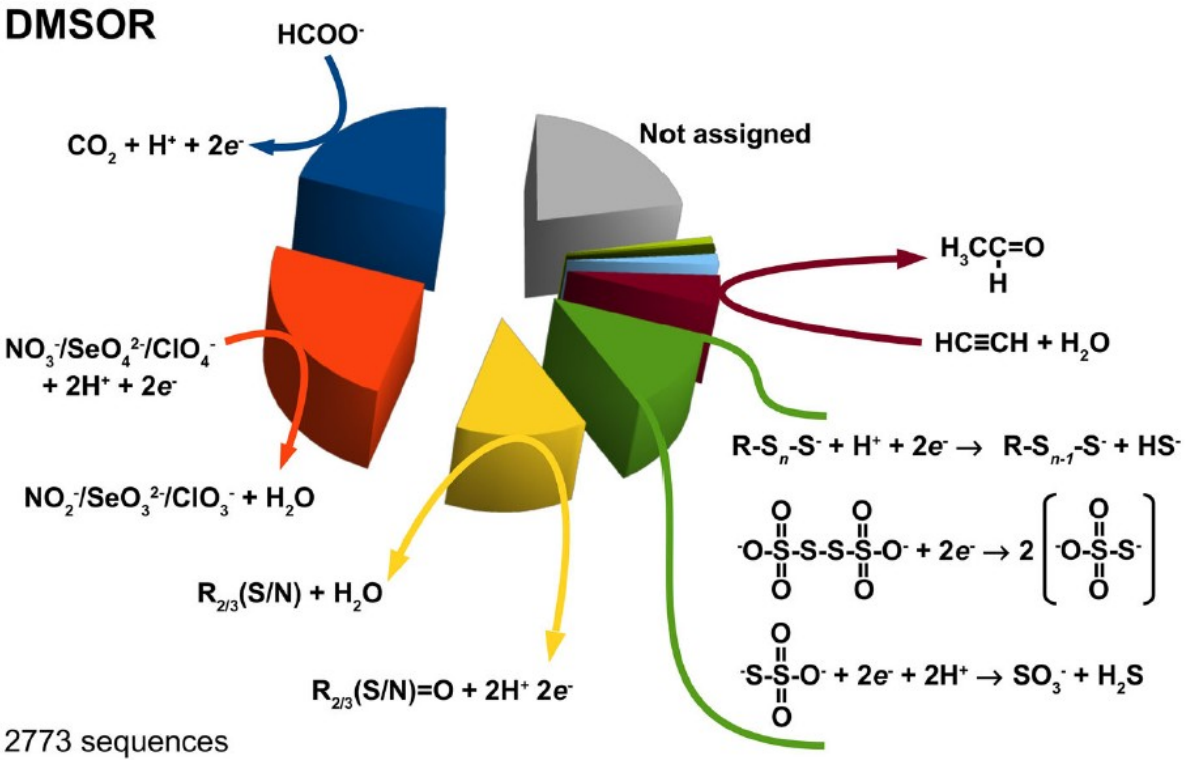

Figure 1.7. DMSOR family functional distribution

The functional distribution of DMSOR family is most diverse among the four groups of molybdoenzymes. A significant portion of DMSOR family members have identified functions. The ones with most representations are formate oxidation, nitrate/selenate/perchlorate reduction, S-/N- oxide oxidoreduction, and sulfur compound oxidoreduction illustrated in blue, orange, yellow, and green, respectively. There are many other functions with smaller representation in the family. Grey area represents DMSOR family with unknown functions. The figure is adapted from Rothery *et al*. (2015) (44).

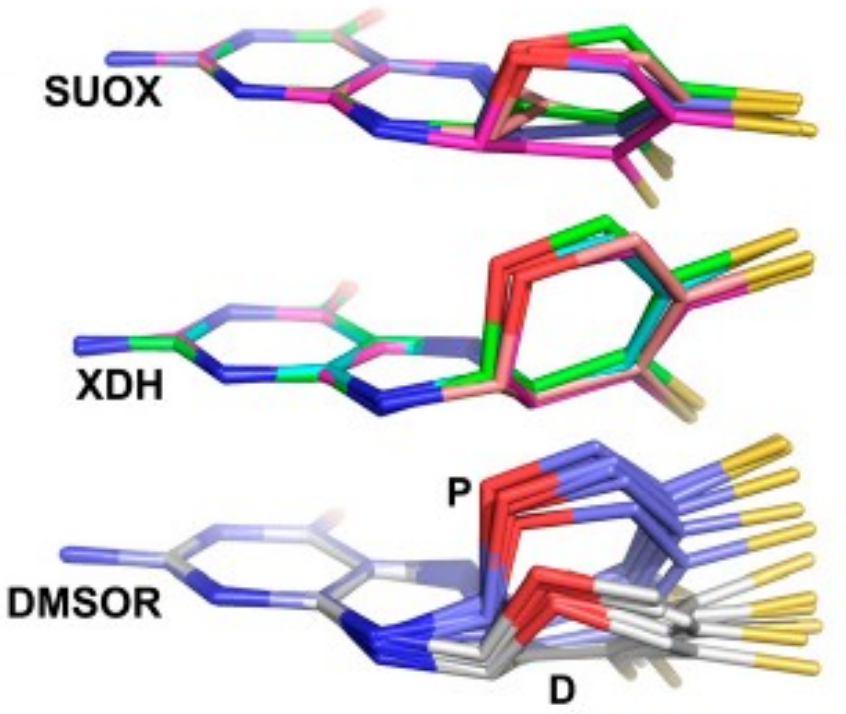

Figure 1.8. Molybdenum cofactor conformational alignment

The structures above are obtained from the available structural information from the Protein Data Bank. The figure illustrates structure conformational difference between the pyranopterins from different molybdoenzyme families. The cofactor from SUOX family is less distorted than that from XDH family, and mostly resembles DMSOR distal pyranopterin. The XDH family molybdenum is more similar to the proximal pyranopterin of a DMSOR Mo-bisPGD. The figure is adapted from Rothery *et al*. (2012) (76).

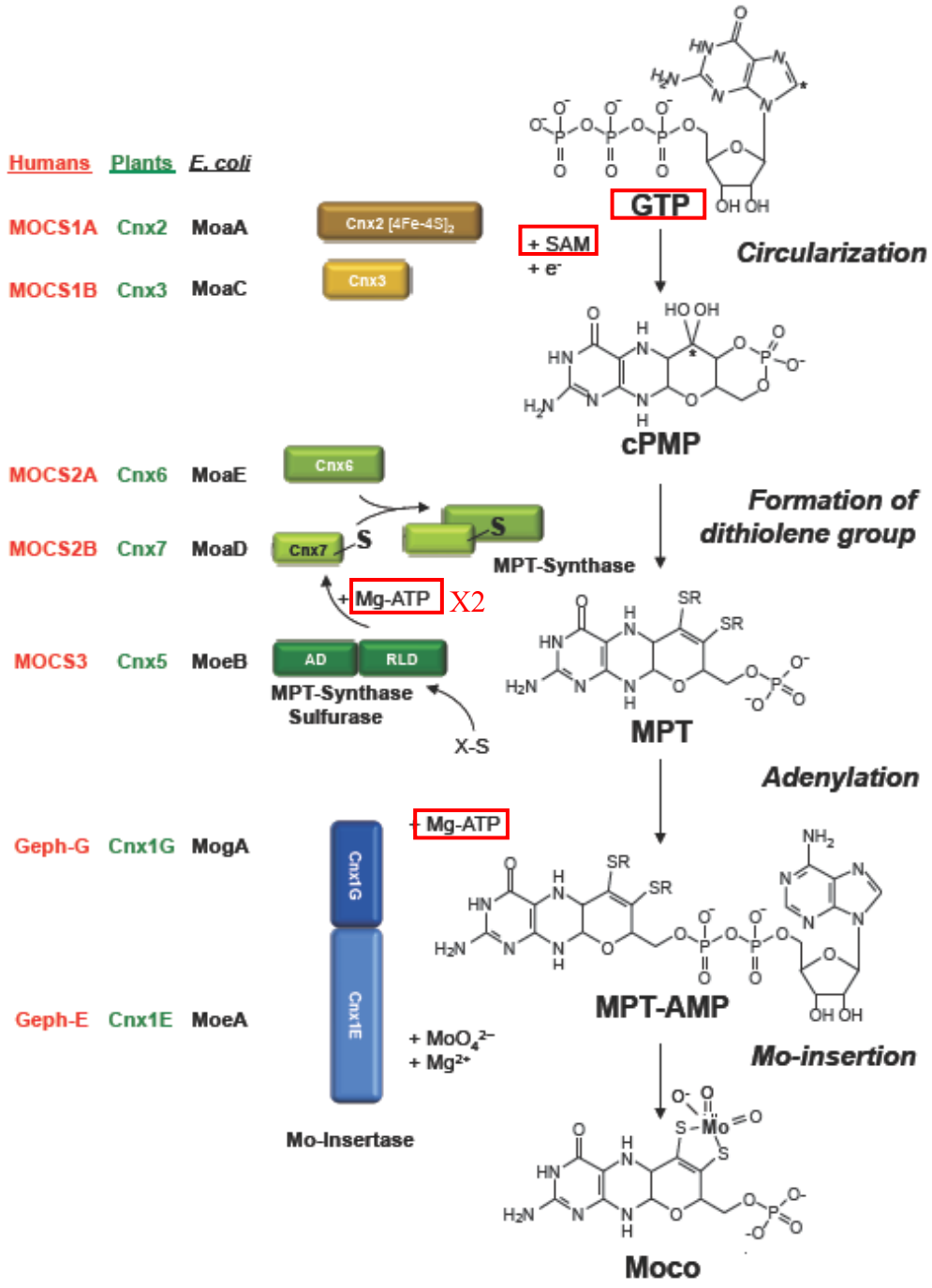

Figure 1.9. Molybdenum cofactor biosynthetic pathway

The figure illustrates four basic steps in the Moco biosynthesis pathway: circularization of GTP, formation of dithiolene on cPMP, adenylation of MPT, and Mo insertion. The enzymes catalyzing those steps are shown on the left side with red represents human enzymes, green represents plant enzymes, and black represents bacterial enzymes. The ATP equivalent molecules are squared in red. There are minimum five ATP equivalent molecules consumed for synthesis of each pyranopterin. The figure is adapted from Mendel. (2013) (63).

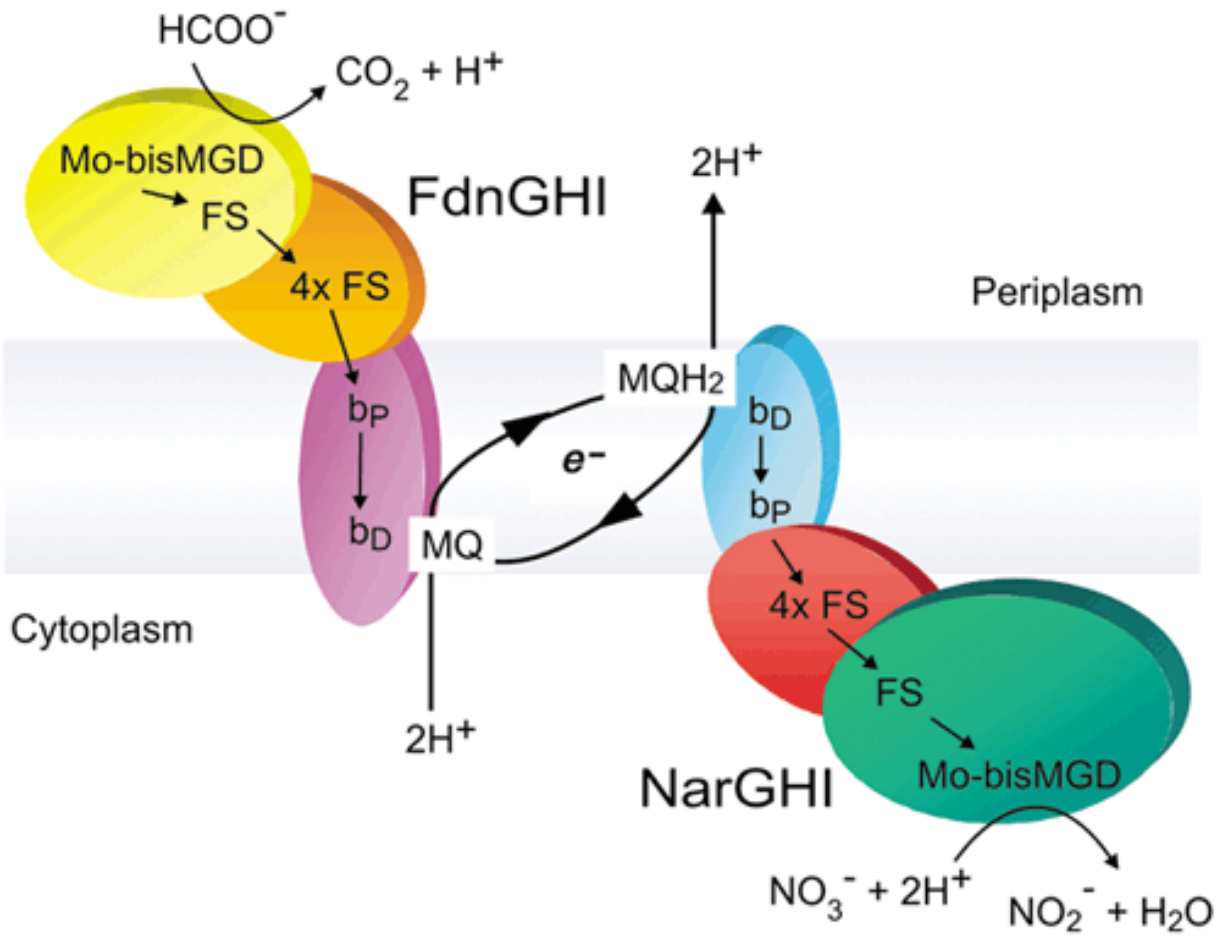

Figure 1.10. Redox loop formed by nitrate reductase and formate dehydrogenase

The figure illustrates the redox loop formed by formate dehydrogenase and nitrate reductase A. FdnGHI converts formate to carbon dioxide and reduces MQ to MQH_2, while NarGHI oxidizes MQH_2 to MQ and uses the two electrons to convert nitrate to nitrite. There is a net seven-proton difference produced in each cycle of the redox loop. The loop is one of the mechanisms allowing *E. coli* to survive anaerobically. The figure is adapted from Bertero *et al.* (2003) (78).

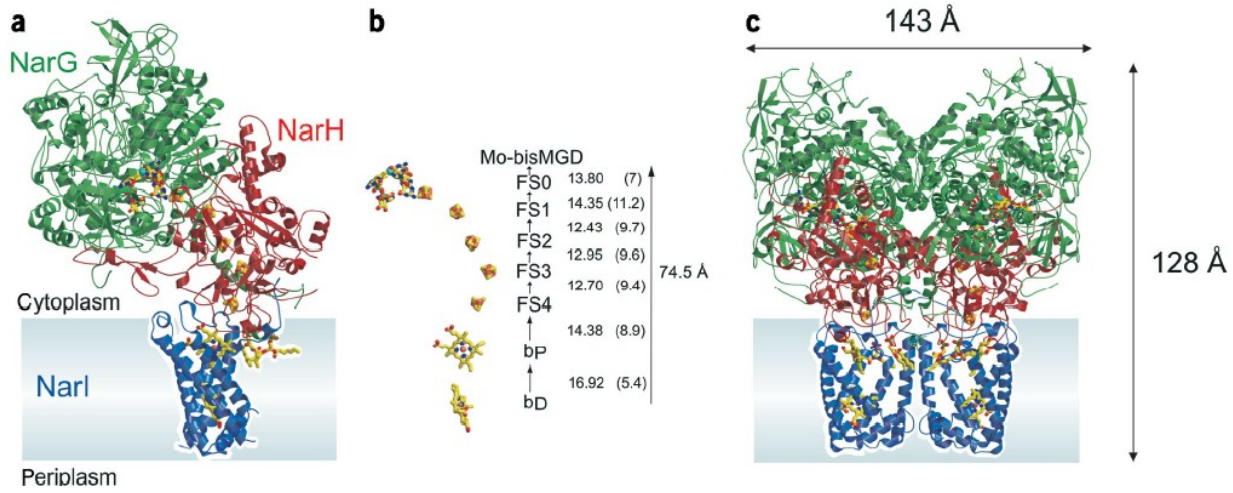

Figure 1.11. Crystal structure of NarGHI (1Q16)

(a) The overall crystal structure of a NarGHI protein. The protein is membrane-bound and faces the cytoplasm. The green represents NarG, the catalytic subunit; the red represents NarH, the electron transfer subunit; and the blue represents NarI, the membrane anchor subunits. There are eight prosthetic groups shown in sticks: Mo-bisPGD and FS0 from NarG, FS1 to FS4 from NarH, Heme b_P and Heme b_D from NarI. Mo, Fe, and S are labelled as cyan, orange, and yellow spheres, respectively. (b) The prosthetic groups are shown in the same position and orientation as in (a). The center-to-center and edge-to-edge (in parenthesis) distances between adjacent prosthetic groups are labelled on the right hand side. (c) NarGHI is in the form of dimers in crystal structures. The dimension of a dimer is 143 Å by 128 Å. The monomers in the diagram are ~90° rotation from (a). The figure is adapted from Bertero *et al.* (2003) (78).

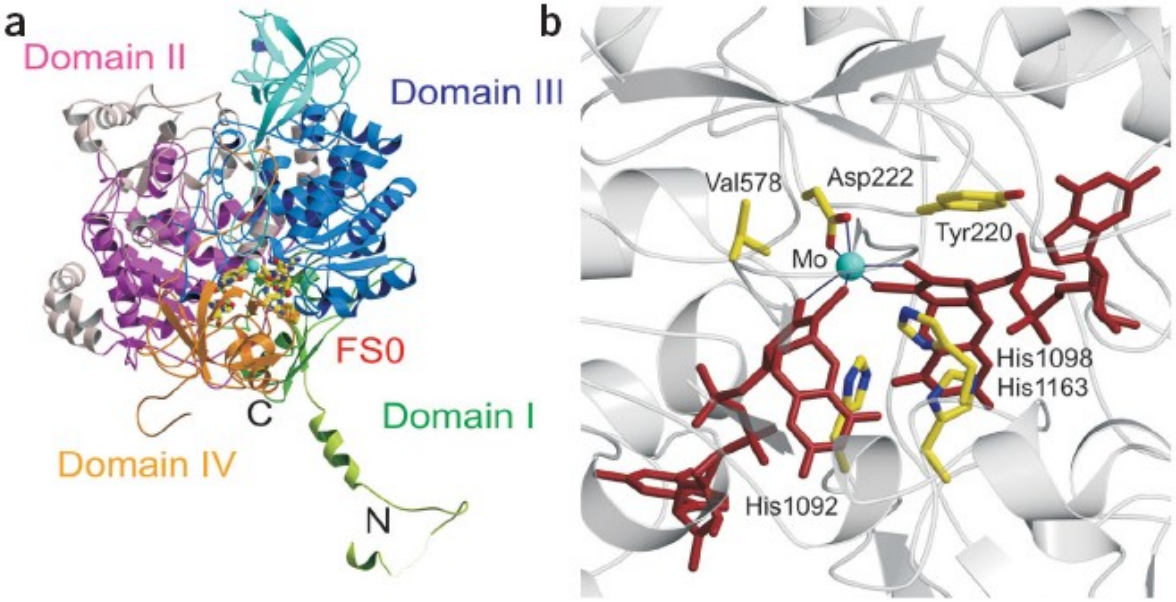

Figure 1.12. NarG structural information

(a) The four domains of NarG are Domain I in green, Domain II in purple, Domain III in blue, and Domain IV in orange. Other structural components are labelled in lighter colors. The molybdenum cofactor is coordinated by domain II and III. Domain I coordinates FSO and contains the extended N terminus that is capable of interacting with other subunits. (b) Detail illustration of the active site Moco with its interacting partners. The molybdenum in a cyan sphere and the cofactor is in red sticks. The residues are yellow sticks with N represented by blue colour. All the residues highlighted are well conserved. The figure is adapted from Bertero *et al.* (2003) (78).

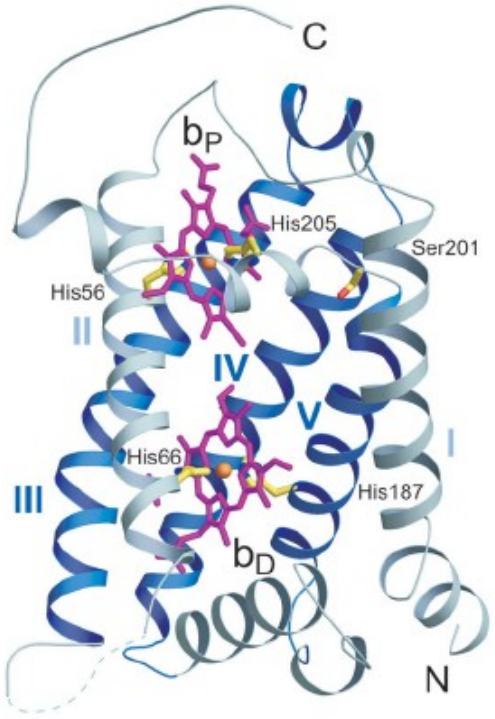

Figure 1.13. NarI structural information

NarI shown in ribbon representation is parallel to the membrane with its five transmembrane helices labelled in grey to blue gradient. The two hemes are in magenta sticks. Fe atoms are in orange sphere and S atoms are in yellow sticks. The histidine coordinating hemes are highlighted. His56 and His205 coordinate Heme b_P; His66 and His187 coordinate Heme b_D. The figure is adapted from Bertero et al. (2003) **(78)**.

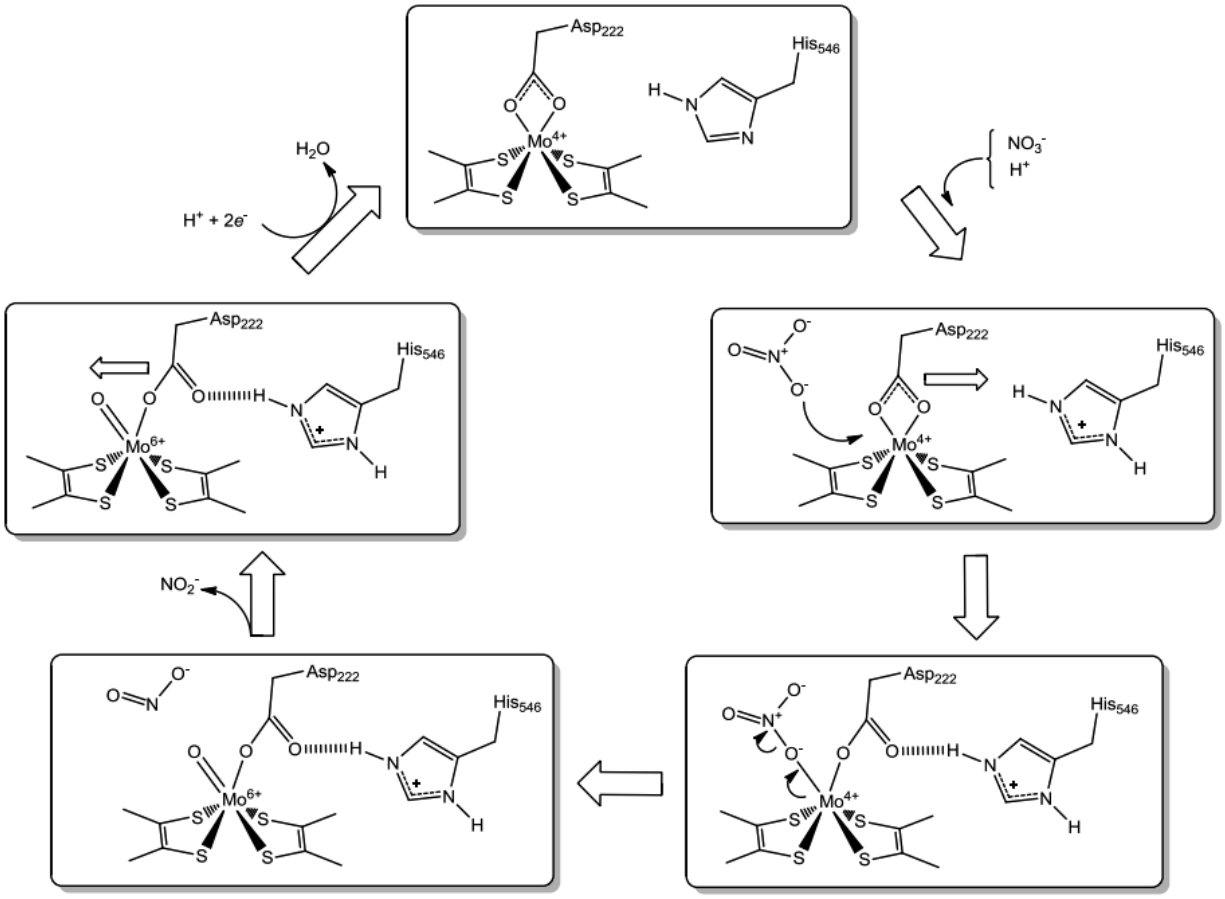

Figure 1.14. The catalytic mechanism of nitrate reduction

The catalytic mechanism proposed by our lab involves Mo atom, NarG-Asp222, and NarG-His546. The Mo(IV) is coordinated by four dithiolene sulfurs and two oxygens from Asp222. The substrate NO_3^- carries out nucleophilic attach onto Mo(IV) and Asp222 switches form the bidentate coordination to a monodentate coordination. The His546 coordinates the Asp carboxyl oxygen that has left the Mo coordination. His546 is further coordinated by Asn1217 which is not illustrated in the figure. Nitrate reduction occurs and Mo is oxidized to +6. Nitrite leaves the Mo center, leaving an oxo group coordinating the Mo(VI). The oxo group leaves as water when Mo is reduced to +4 again and Asp222 re-establish the bidentate coordination. The Figure is created by Dr. Richard Rothery.

CHAPTER 2. Pyranopterin Coordination Controls Molybdenum Electrochemistry in *Escherichia coli* Nitrate Reductase

This work is accepted and published online in August 2015 by *Journal of Biological Chemistry*

Author contributions

Sheng Yi Wu designed, performed and analyzed the experiments presented in the manuscript. Dr. Richard A. Rothery wrote the paper and contributed to the data analyses. Dr. Joel H. Weiner conceived and coordinated the study.

Acknowledgments: This work was funded by the Canadian Institutes of Health Research (Grant MOP15292), the Canada Foundation for Innovation, the Alberta Heritage Foundation for Medical Research, and Natural Science and Engineering Research Council - Collaborative Research and Training Experience Program. We thank Justin Fedor for critical reading of the manuscript, and Shannon Murphy for providing technical support.

2.1 Introduction

Enzymes containing the mononuclear molybdenum cofactor (Mo-enzymes) support an extraordinary diversity of redox transitions spanning a reduction potential range of approximately one volt (10, 123). Their active sites comprise a Mo atom coordinated by one or two pyranopterin dithiolene chelates, with additional metal coordination being provided by oxo/sulfido groups and/or oxygen/sulfur atoms derived from amino acid side chains (124, 125). Mo-enzymes fall into three major families, each of which has a distinct protein fold: the sulfite oxidases and plant nitrate reductases [the SUOX family (68)]; the xanthine dehydrogenases and carbon-monoxide dehydrogenases [the XDH family (126)]; and enzymes related to the bacterial DMSO reductases [the DMSOR family (75, 126)]. The metal atom of the SUOX and XDH families is coordinated by a single pyranopterin dithiolene chelate, whereas in the DMSOR family it is coordinated by two such moieties (44, 75, 126). The situation is further complicated by the presence of a cytosine nucleotide attached via a phosphodiester linkage to the methyl group of the pyranopterin in some members of the XDH family (69), and by the presence of a guanine nucleotide similarly attached to each pyranopterin in members of the DMSOR family (44, 75, 126). The precise function of the pyranopterin component of the molybdenum cofactor remains unclear: it clearly functions as part of the molecular scaffold holding the Mo atom in an optimum position for catalysis (127, 128); and it has recently been proposed that it may also modulate Mo reduction potentials and hence reactivity via alternate oxidation states (e.g. dihydro- versus tetrahydro- oxidation states) (44, 76, 119, 120, 129, 130).

Evolutionary analyses have established the presence of the DMSOR protein fold in the “last universal common ancestor” from which all extant species evolved (131, 132). An important consequence of this is that the fold has evolved to support catalytic functions encompassing

those necessary prior to and after the evolution of oxygenic photosynthetic water oxidation (133). This process likely encompassed substitutions of the protein-metal ligands, modulation of the metal coordination sphere via the bis-dithiolene chelate, and modification of the pyranopterin coordination environment. The DMSOR family is able to support a broad range of redox transitions including the following: oxidation of formate, arsenite, ethylbenzene, and dimethylsulfide; and the reduction of polysulfide, nitrate, chlorate, trimethylamine-N-oxide and dimethylsulfoxide (44, 75, 123, 126). A plausible hypothesis explaining the presence of the second pyranopterin in the DMSOR family is that it adds additional facets of fine tuning to facilitate reactivity towards the observed broad range of substrates. The pyranopterin coordination environments may play a critical role in modulating dithiolene chelate electrostatics via differences in hydrogen bonding environment, conformation, and oxidation state (44, 76, 119–121, 130, 134). While much attention has been paid to the role of the immediate metal environment in defining catalysis (66, 128, 135, 136), little is known about the role of the pyranopterin coordination environment.

The molybdenum cofactor found in the DMSOR family is a molybdo-bis(pyranopterin guanine dinucleotide) (Mo-bisPGD) (44, 75, 123, 126). The pyranopterins are referred to as proximal and distal based on their positions relative to a conserved [4Fe-4S] cluster, known as FS0, that is present in almost every member of the DMSOR enzyme family. In enzymes for which high-resolution structures are available, the proximal pyranopterin has a more distorted conformation than that of the distal pyranopterin, consistent with the former being in a fully-reduced tetrahydro-form; and with the latter having accessibility to the partially-oxidized 10,10a dihydro form (76). In two members of the family, *Escherichia coli* respiratory nitrate reductase (NarGHI) (78) and *Aromatoleum aromaticum* ethylbenzene dehydrogenase (EbdABC) (77), high-

resolution protein structures reveal that the distal pyranopterin has a bicyclic structure with an open pyran ring[1]. These observations raise the question of the role of the alternate open pyran ring structure in defining active site redox chemistry and catalysis. In the case of NarGHI, protein crystallography reveals that the open pyran ring oxygen participates in hydrogen bonding interactions with two conserved residues in NarG: NarG-His1163 and NarG-Ser719 [((125) **Figure 2.1 A**)]. The distances between the Ser719 OG proton and the pyran oxygen and between the His1163 NE2 proton and the pyran oxygen are both approximately 2 Å. Closer inspection reveals the presence of a second conserved His residue (NarG His1184) that completes a charge-transfer relay connecting the pyran oxygen with three structurally-conserved water molecules at its distal end (**Figure 2.1**). It would therefore be of interest to generate variants of NarG-Ser719, His1163, and His1184 and determine their effects on Mo electrochemistry and catalysis.

We recently examined the coordination environment of the pyranopterin piperazine nitrogens in members of the DMSOR family for which high-resolution structures are available (44, 76), revealing that all members of the family contain a His or Arg residue that bridges the two piperazine N-5 atoms. With the exception of the *Thermus thermophilus* polysulfide reductase (137), all DMSOR fold enzyme structures obtained to date contain an additional residue (a His/Ser/Gln) that stabilizes the N-5 of the proximal pyranopterin in an sp3 hybridized state. **Figure 2.2 A** illustrates piperazine nitrogen coordination of the NarGHI pyranopterins. The N-10 atoms of both piperazines are hydrogen-bond donors to backbone amide oxygens (of NarG Thr259 and NarG Ser720). The N-5 atoms are bridged by the imidazole of NarG His1092, with the N-5 atom of the proximal pyranopterin participating in an additional H-bond with the NE2 nitrogen of NarG His1098. These two residues are referred to as the "bridging" and "stabilizing"

[1] The bicyclic form is therefore formally a pterin rather than a pyranopterin. However, for the sake of brevity, it is referred to as a pyranopterin herein.

histidines, respectively, and their H bonding contacts are summarized in **Figure 2.2 B**. That almost all of the proximal N-5 atoms in the DMSOR family have two hydrogen bonding contacts favors a tetrahydro oxidation state for the proximal pyranopterin. The single H-bonding contact observed for the N-5 atoms of all the distal pyranopterins provides further support for the suggestion that these have accessibility to the 10,10a-dihydro oxidation state (44, 76). In some members of the DMSOR family, [e.g. *E. coli* formate dehydrogenase N (FdnGHI (138)) and the periplasmic nitrate reductase from *Cupriavidus necator* (NapAB (139))], the bridging ligand is an Arg residue. It would therefore be of interest to generate variants of His1092 and His1098 and determine their effects on Mo electrochemistry and catalysis.

In this paper, we tested the hypothesis that the pyranopterins of the DMSOR family of molybdoenzymes have a non-innocent role in defining Mo electrochemistry and catalysis. If the role of the pyranopterin dithiolene chelates is merely to contribute to a Mo-binding scaffold at the active site, then variants of the target residues studied herein should have little or no effect on enzyme function. If, however, the non-innocence reported for model compounds extends beyond the dithiolene chelate and into the heterocyclic ring system of the pyanopterin (76, 119–121), variants of pyranopterin-coordinating residues should have a dramatic effect on molybdenum electrochemistry and catalysis.

2.2 Experimental procedures

2.2.1 Bacterial strains and plasmids

E. coli LCB79 (araD139 Δ(lacIPOZYA-argF) rpsL, thi Ø79(nar-lac)) (140) was used as the host for all the experiments described herein. NarGHI was expressed from the plasmid pVA700 (141).

2.2.2 Site-directed mutagenesis

Mutant plasmids were generated using the QuikChange site-directed mutagenesis kit from Stratagene. DpnI was purchased from Invitrogen, and DNA purification kits were purchased from Qiagen. Mutants were verified by DNA sequencing (DNA Core Facility, Department of Biochemistry, University of Alberta). Preparation of competent cells and their transformations with plasmids were carried out as previously described (142).

2.2.2.1 Generation of a NarG-Ser719Ala variant

A 4.5 kbp SacI-AvaI fragment of pVA700 was subcloned into pTZ18R and the resultant plasmid was used for site-directed mutagenesis. A 3.3 kbp SacI-NcoI fragment was cloned back into the pVA700 expression vector, creating pVA700/Ser719Ala.

2.2.2.2 Generation of NarG-His1163Ala and NarG His1184Ala variants

A 4.6 kbp EcoRI-SacII fragment of pVA700 was subcloned into pBlueScript to generate a template for site-directed mutagenesis. A 2.1 kb NcoI-SacII fragment was cloned back into the pVA700, creating pVA700/His1163Ala or pVA700/His1184Ala.

2.2.2.3 Generation of NarG-His1092Ala, NarG-His1092Arg, and NarG-His1098Ala variants

The EcoRI-SacII fragment cloned into pBluescript was used as a site-directed mutagenesis template, after which a 1.2 kbp NcoI/BstBI fragment was cloned back into the pVA700, creating pVA700/His1092Ala, pVA700/His1092Arg, or pVA700/His1098Ala.

2.2.3 Growth of cells

Cells were grown microaerobically in 2 L batch cultures of Terrific Broth (142) at 30 °C in the presence of 100 μg mL^{-1} streptomycin and ampicillin. A 10 % innoculum of a stationary phase culture was used and NarGHI overexpression was induced by addition of 0.2 mM isopropyl-1-thio-β-D-galactopyranoside (IPTG). Following addition of the innoculum and IPTG, cells were grown overnight with gentle shaking, and were harvested by centrifugation, and subsequently washed in a buffer containing 100 mM MOPS and 5 mM EDTA (pH 7.0). Cells were resuspended in buffer, and phenylmethylsulfonyl fluoride was added to a final concentration of 0.2 mM. Cell lysis was achieved by three passages through an Emulsiflex C3 microfluidizer (Avestin) at a pressure of 17,000 p.s.i. Crude membranes were prepared by differential centrifugation as previously described (143). These were resuspended in buffer and layered on top of a 55% (w/v) sucrose step (made up in buffer). Following ultracentrifugation at 40,000 r.p.m. for 1.5 hours, the floating band enriched in cytoplasmic membrane vesicles was collected. Excess sucrose was removed by two dilution and ultracentrifugation steps. The final membrane pellet was resuspended in buffer to a concentration of approximately 30 mg mL^{-1}, and were flash frozen in liquid nitrogen prior to being stored at -70 °C until use. Where appropriate, buffer exchange prior to EPR analysis was achieved by dilution and re-centrifugation. Overexpression of NarGHI was evaluated by polyacrylamide gel electrophoresis (144).

2.2.4 Bacterial growth on glycerol-nitrate minimal medium

Anaerobic growth of *E. coli* harboring LCB79/pVA700 and mutant derivatives was assessed in a glycerol-nitrate (GN) minimal medium essentially as previously described (145, 146). Nitrate was added (as KNO_3) to a final concentration of 40 mM. Growth was evaluated at 37 °C, and

culture turbidity was measured using a Klett-Summerson spectrophotometer equipped with a No. 66 filter. Maximal growth rates were calculated as described by Zwietering et al. (147), and were expressed as the parameter μm in units of (Klett units) hour^{-1}.

Form A fluorescence of the pyranopterin cofactor. Pyranopterin was assayed by generation of its Form A fluorescent derivative following protein denaturation (148, 149), essentially as previously described (146). As starting material, 10 mg of membrane protein were used.

2.2.5 Redox potentiometry and EPR spectroscopy

Redox titrations were carried out under argon at 25 °C as previously described (150, 151) in 100 mM Tricine and 5 mM EDTA (pH 8.0). The protein concentration used was approximately 30 mg mL $^{-1}$. The following redox mediators were used at a concentration of 25 μM: quinhydrone, 2,6-dichloroindophenol, 1,2 naphthoquinone, toluylene blue, phenazine methosulfate, thionine, methylene blue, resorufin, indigotrisulfonate, indigocarmine, anthraquinone-2-sulfonic acid, phenosafranine, and neutral red. All samples were prepared in quartz EPR tubes with a 3 mm internal diameter, and were rapidly frozen in liquid nitrogen-chilled ethanol and stored at 77 K until use. EPR spectra were recorded at 150 K using a Bruker Elexsys E500 spectrometer equipped with a Bruker SHQE microwave cavity and a Bruker ER4131 Variable Temperature Unit using liquid nitrogen as a cryogen. Potentiometric titration data were analyzed by plotting the intensity of the molybdenum peak-trough versus E_h and fitting the data to two E_m values (E_1 and E_2) (152). Mo(V) stability constants (K_{stab}) were calculated as described by Ohnishi et al. (153). Fitting was performed using the Solver for Nonlinear Programming extension of Libre Office Calc. Where appropriate the statistical significance of differences in E_m values was evaluated using a t-test.

2.2.6 Protein assays

Protein concentrations were assayed as described by Lowry et al. (154) modified by the inclusion of 1% (w/v) sodium dodecyl sulfate in the incubation mixture to solubilize membrane proteins (155).

2.2.7 Enzyme Assays

Nitrate reductase activities were measured using the non-specific electron donor benzyl viologen (33). Assays were carried out at pH 8.0 in a buffer containing 100 mM Tricine, 0.23 mM benzyl viologen, 5 mM EDTA and 4 mM KNO_3. Benzyl viologen was reduced by adding an excess of sodium dithionite (approximately 0.4 mM), and the reaction was initiated by addition of a catalytic amount of enzyme.

2.3 Results and discussion

2.3.1 Residues targeted for site-directed mutagenesis

During nitrate reduction, the Mo atom of the Mo-bisPGD cycles through the IV, V, and VI oxidation states to catalyze the two electron reduction of nitrate to nitrite (156). To investigate the effect of pyranopterin coordination on Mo electrochemistry, we generated variants of two sets of pyranopterin-coordinating residues in NarG: (i) those interacting directly or indirectly with the oxygen of the open pyran ring of the distal pyranopterin (NarG-Ser719, NarG-His1163 and NarG-His1184; **Figure 2.1**); and (ii) those involved in bridging the proximal and distal pyranopterins and stabilizing the oxidation state of the proximal pyranopterin (NarG-His1092 and NarG His1098; **Figure 2.2**). As judged by SDS-PAGE and Form A pyranopterin assays,

each variant was expressed in a Mo bisPGD-containing form at levels comparable to that of the wild-type. We used these variants to test the hypothesis that residues coordinating the pyranopterin moiety of the Mo bisPGD cofactor play a critical role in defining molybdenum electrochemistry and substrate reactivity.

2.3.2 Impact of the variants on the NarG Mo(V) EPR spectrum

Of the three accessible Mo oxidation states, only the intermediate Mo(V) state is paramagnetic and EPR-visible. It can be observed in spectra recorded of samples poised at appropriate reduction potentials. Because the NarGHI Mo(V) signal is sensitive to pH in an anion-dependent way (157, 158), we recorded spectra of samples poised at pH8.0, wherein the so-called "high pH" form is dominant. This form exhibits a simple rhombic EPR spectrum with an absence of resolved hyperfine (1H) couplings (157) that simplifies subsequent analyses of potentiometric data (see below).

Figure 2.3 A shows spectra of redox-poised samples containing variants of residues implicated in coordinating the open pyran oxygen of the distal pyranopterin (Ser719Ala, His1163Ala and His1184Ala). In general, these spectra are similar to those previously observed for the Mo(V) species of NarGHI (150, 157, 158), wherein a spectrum of a rhombic Mo(V) species is observed with $g_{1,2,3}$ values of approximately 1.988, 1.982, and 1.962. As was the case in previous studies (157–159), no hyperfine coupling was resolved with the isotopes of Mo having a nuclear spin of 5/2 (95Mo and 97Mo, with natural abundances of ~16 % and 10 %, respectively). These data indicate that the Ser719Ala, His1163Ala and His1184Ala variants do not significantly impact the Mo coordination sphere.

Figure 2.3 B shows spectra of redox-poised samples of variants of residues implicated in bridging the two pyranopterins (His1092Ala and His1092Arg), or stabilizing the proximal pyranopterin in its tetrahydro form (His1098Ala). Of these, the His1092Ala variant has the most dramatic effect on the Mo(V) EPR spectrum, shifting g_2 upfield from approximately g = 1.982 (wild-type) to approximately g = 1.962 (His1092Ala). The His1092Arg variant exhibits an EPR spectrum wherein heterogeneity is observed, especially in the g_3 feature. Finally, the His1098Ala variant exhibits a spectrum with clearly defined $g_{1,2,3}$ values, with greater rhombicity than that of the wild-type. Overall, Mo(V) species are clearly visible in all of the NarGHI variants studied herein, with the His1092Ala variant having the greatest effect on the Mo(V) EPR spectrum (see below).

2.3.3 Influence of the NarGHI variants on Mo electrochemistry

Molybdenum redox cycling is defined by two reduction potentials, E_1 and E_2, corresponding to the Mo(VI/V) and Mo(V/IV) reduction potentials, with the average of these being defined as the overall reduction potential (E_m). The difference between E_1 and E_2 is a reflection of the stability of the intermediate Mo(V) species, and can be used to calculate its stability constant (K_{stab}) (153). We performed potentiometric titrations on all the variants of NarGHI studied herein, and in each case titrations were carried out on samples generated from 3-4 independent biological replicates. **Figure 2.4-A** shows representative titrations for the variants of residues interacting with the O-1 pyran oxygen (**Figure 2.1**). **Figure 2.4 B** shows plots of the residuals between the experimental data and the fits. For the wild-type enzyme, we estimate values of E_m and K_{stab} of 142 mV and 28, respectively (summarized in **Figure 2.4 C**). These values are in reasonable agreement with those previously obtained (150, 160–162). The Ser719Ala variant has a statistically-insignificant effect on the E_m (ΔE_m = 4 mV, P = 0.57) and decreases the K_{stab} from 28 to 8, while the His1163Ala

variant elicits a large decrease in the E_m ($\Delta E_{\mathbf{m}}$ = -88 mV, **Table 2.1**) and a concomitant decrease in the K_{stab} from 28 to 1. The His1184Ala variant has an intermediate effect, eliciting a ΔE_m of -36 mV, and decreases the K_{stab}, again from 28 to 1. Thus, the charge-transfer relay depicted in **Figure 2.1 B** appears to play two critical roles: (i) modulating the Mo reduction potentials (see below for further discussion of this); and (ii) stabilizing the Mo(V) intermediate.

Figure 2.5 A shows representative potentiometric titrations of the His1092Ala, His1092Arg, and His1098Ala variants. The His1092Arg variant replaces the bridging His residue with an Arg, and mimics the pyranopterin-coordination environment observed in the formate dehydrogenases and periplasmic nitrate reductases [e.g. FdnGHI and NapAB, respectively (44)]. The His1092Arg variant elicits a modest increase of marginal statistical significance in the overall Mo E_m (ΔE_m = 18 mV, P = 0.07; **Table 2.1**), consistent with there being no change in overall charge of the bridging residue when it is changed from a His to an Arg (the pK_a of the Arg guanidinium group is approximately 12.5). This suggests that the imidazole pK_a is significantly increased from approximately 6.0 in aqueous solution to > 8.0 in the bridging environment between the two pyranopterins. The His1092Ala variant elicits a ΔE_m on the Mo center of approximately -143 mV along with a modest decrease in its K_{stab} (from 28 to 19, **Table 2.1**). A possible explanation for the large negative ΔE_m is that the void between the two pyranopterins contains waters in the His1092Ala variant, and that these waters lack an overall positive charge, thus decreasing the overall Mo reduction potential. Alternatively, given that the His1092Ala variant has the most severe effect on the Mo(V) EPR spectrum, loss of "scaffolding" by the bridging imidazole moiety may result in a significant alteration of the geometry of dithiolene coordination that may cause the large observed ΔE_m.

The His1098Ala variant elicits a ΔE_m of 101 mV, along with a significant increase in Mo(V) stability, with the K_{stab} increasing from 28 to 1822 (**Figure 2.5 A** and **2.5 C**, **Table 2.1**). **Figure 2.2 B** shows a model for how His1092 and His1098 define the H bonding environment of the proximal pyranopterin piperazine N-5 atom. As suggested above, formal protonation of the imidazole of His1092 is supported by the relative lack of effect of the His1092Arg variant on the overall Mo E_m. One of the H-bonds is eliminated in the His1098Ala variant, which may result in transfer of the proton from the ND1 atom to the piperazine N-5, resulting in loss of a positive charge and the observed decrease in the overall Mo E_m.

We proposed that in the DMSOR family of enzymes, the role of the stabilizing residue (His1098 in NarG) is to maintain the N-5 atom of the proximal pyranopterin in an *sp*3-hybridized form, thus stabilizing the tetrahydro oxidation state (44, 76). This suggests a possible explanation for the observed increase in Mo(V) stability in the His1098Ala variant. Removal of the hydrogen-bonding contact provided by the His1098 imidazole may result in the 10,10a dihydro oxidation state becoming available to the proximal pyranopterin. If the 10,10a dihydro to tetrahydro reduction potential occurs within the range in which Mo(V) is extant, then E_1 (the Mo(VI/V) reduction potential) could be shifted to the observed value of 139 mV (**Table 2.1**; see reference (76)).

2.3.4 Correlation between enzyme activity, cell growth and Mo electrochemistry

How do changes in Mo electrochemistry impact enzyme activity and anaerobic respiratory growth on nitrate? Specific activities in enriched membranes for the variants studied herein range from 1 to 54 μmoles min^{-1} mg^{-1} for the His1092Ala and Ser719Ala variants, respectively (**Table**

2.1). With the exception of the His1092Arg variant, a strong correlation exists between overall Mo reduction potential and enzyme activity (R = 0.99, **Figure 2.6**). A correlation also exists between respiratory growth rate and Mo reduction potential across all variants (R = 0.95, inset to **Figure 2.6**). Thus, catalysis and growth are convincingly correlated with increased Mo E_m. A possible explanation for this is that catalytic turnover depends on the energetics of electron transfer from FS0 (E_m = -55 mV (161)) to the Mo.

It is notable that NarGHI catalytic activity appears to be dependent on the overall Mo E_m, but not on the Mo(V) K_{stab} (**Table 2.1**). Protein film voltammetry studies of NarGHI (156) and two other members of the DMSOR family (the periplasmic nitrate reductase from *Rhodobacter sphaeroides*, NapAB (163), and the Me_2SO reductase from *E. coli* (164) demonstrated that enzyme turnover decreases below a reduction potential referred to as E_{switch}. It was therefore proposed that observation of an E_{switch} arises because substrate binds preferentially to the Mo(V) form of the cofactor (156, 163, 164). In the case of NarGHI, this is corroborated by the observation of a stable nitrate adduct to the Mo(V) (158). If the mechanism of nitrate reduction proceeds via substrate binding to a Mo(V) species, we would expect a variant that increases the Mo(V) K_{stab} to retain significant catalytic activity. The His1098Ala variant exhibits a very large Mo(V) K_{stab} (~1822; **Table 2.1**), but has low specific activity and growth rate compared to the wild-type (**Figure 2.6**).

As previously noted (76), an alternative explanation for the observed E_{switch} is that it controls a reduction of the distal pyranopterin from an oxidation state equivalent to the 10,10a-dihydro form to one equivalent to the tetrahydro form. This provides a possible explanation for why the His1092Arg variant supports respiratory growth on nitrate, but has decreased enzyme activity in our *in vitro* assay (**Figure 2.6**). It is possible that a significant positive ΔE_m is elicited on the

E_{switch}, resulting in lower activity measured using benzyl viologen as electron donor (E_m = -374 mV (165)). NarGHI is able to function *in vivo* with either ubiquinol or menaquinol as electron donor (166), and these have reduction potentials of +110 and -80 mV, respectively (10), rendering them both less likely to reduce the distal pyranopterin than the artificial electron donor benzyl viologen.

2.3.5 Role of the His1163/His1184 charge-transfer relay in NarGHI maturation and in modulation of Mo electrochemistry

NarGHI maturation is a carefully orchestrated process involving the NarJ system-specific chaperone (167) and the twin arginine translocase (168). In general, the process ensures assembly of correctly folded enzyme with a complete complement of cofactors (167, 169). Insertion of the Mo-bisPGD cofactor depends on the presence of the FS0 [4Fe-4S] cluster (167, 169). With the exception of EbdABC (77), NarGHI is the only enzyme examined to date that has a bicyclic distal pyranopterin (78). Closer examination of the charge-transfer relay comprising His1163 and His1184 (**Figure 2.1**) suggests a possible mechanism for pyran ring opening (**Figure 2.7**), which proceeds as follows. The His1163/His1184 charge-transfer relay catalyzes elimination of the C-4a proton (**Figure 2.7 A**), generating an open ring-form with a piperazine ring in a form equivalent to the 5,10-dihydro form (**Figure 2.7 B**) in a mechanism essentially identical to that previously described (170). This form rearranges to the lowest energy tautomer (equivalent to the 10,10a-dihydro form (76, 170)) shown in **Figure 2.7 C**. A mechanism essentially identical to that presented in **Figure 2.7 A-C** can be proposed for ring-opening of the distal pyranopterin in EbdABC, with the distinction that ring opening would be catalyzed by a guanidinium side chain rather than by an imidazole. The equilibrium between the structures

shown in **Figure 2.7 C** and **2.7 D** illustrates how the formal change on the pyran oxygen (and the overall Mo reduction potential) can be modulated by the His1163/His1184 charge-transfer relay. Stabilization of the pyran oxygen in its alkoxide form would decrease the overall Mo reduction potential, whereas formal protonation to the hydroxyl form would increase the overall Mo reduction potential.

In the context of the model presented in **Figure 2.7 C** and **2.7 D** for charge-transfer induced Mo reduction potential modulation, it is notable that the His1163Ala variant elicits a large ΔE_m that is approximately double that elicited by the His1184Ala variant. This is consistent with the entire charge transfer relay being involved in Mo reduction potential modulation. It is possible to speculate that the His1163Ala variant may impact an equilibrium between the open and closed pyran ring forms of the distal pyranopterin, and we are currently addressing this issue using protein crystallography.

2.4 Conclusion

We have demonstrated the importance of the pyranopterin coordination environment in defining Mo electrochemistry and substrate reactivity, with enzyme activity correlating with increasing overall Mo reduction potential. Our studies demonstrate the importance of factors beyond the immediate Mo coordination sphere in defining enzyme activity.

2.5. Table

Table 2.1. Effects of variants of pyranopterin-coordinating residues on Mo reduction potentials and enzyme activity

Variant	E_m (mV)[a]	ΔE_m (mV)[b]	E_1 (mV)[c]	E_2 (mV)[d]	K_{stab}	Maximal growth rate, μ_m ((Klett units) hr^{-1})	$BV^{\cdot -}$:NO_3^- activity (μmoles min^{-1} mg^{-1})
Wild-type	142 ± 12 (n = 4)	0	184 ± 10	99 ± 16	28	15.4 ± 0.7 (n = 3)	48 ±14 (n = 3)
Ser719Ala	146 ± 7 (n = 3)	4	170 ± 19	122 ± 7	8	15.5 ± 0.9 (n = 3)	54 ±11 (n = 3)
His1163Ala	54 ± 3 (n = 4)	-88	53 ± 5	54 ± 9	1	6.1 ± 0.2 (n = 3)	23 ± 4 (n = 3)
His1184Ala	106 ± 5 (n = 3)	-36	106 ± 14	106 ± 5	1	11.4 ± 0.6 (n = 3)	36 ± 1 (n = 3)
His1092Ala	-1 ± 3 (n = 3)	-143	35 ± 9	-38 ± 11	19	4.4 ± 0.5 (n = 2)	0.9 ± 0.1 (n = 3)
His1092Arg	160 ± 7 (n = 3)	18	225 ± 15	95 ± 2	171	12.8 ± 0.4 (n = 2)	8.6 ± 0.6 (n = 3)
His1098Ala	41 ± 4 (n = 4)	-101	139 ± 7	-57 ± 2	1822	4.8 ± 0.5 (n = 2)	16 ± 2 (n = 3)

[a] – Overall Mo(VI/V/IV) reduction potential at pH 8.0.

[b] – E_m (variant) *minus* E_m (wild-type). Where appropriate, P values indicating the statistical significance of each ΔE_m are given in the text.

[c] – Mo(VI/V) reduction potential.

[d] – Mo(V/IV) reduction potential.

2.6. Figures

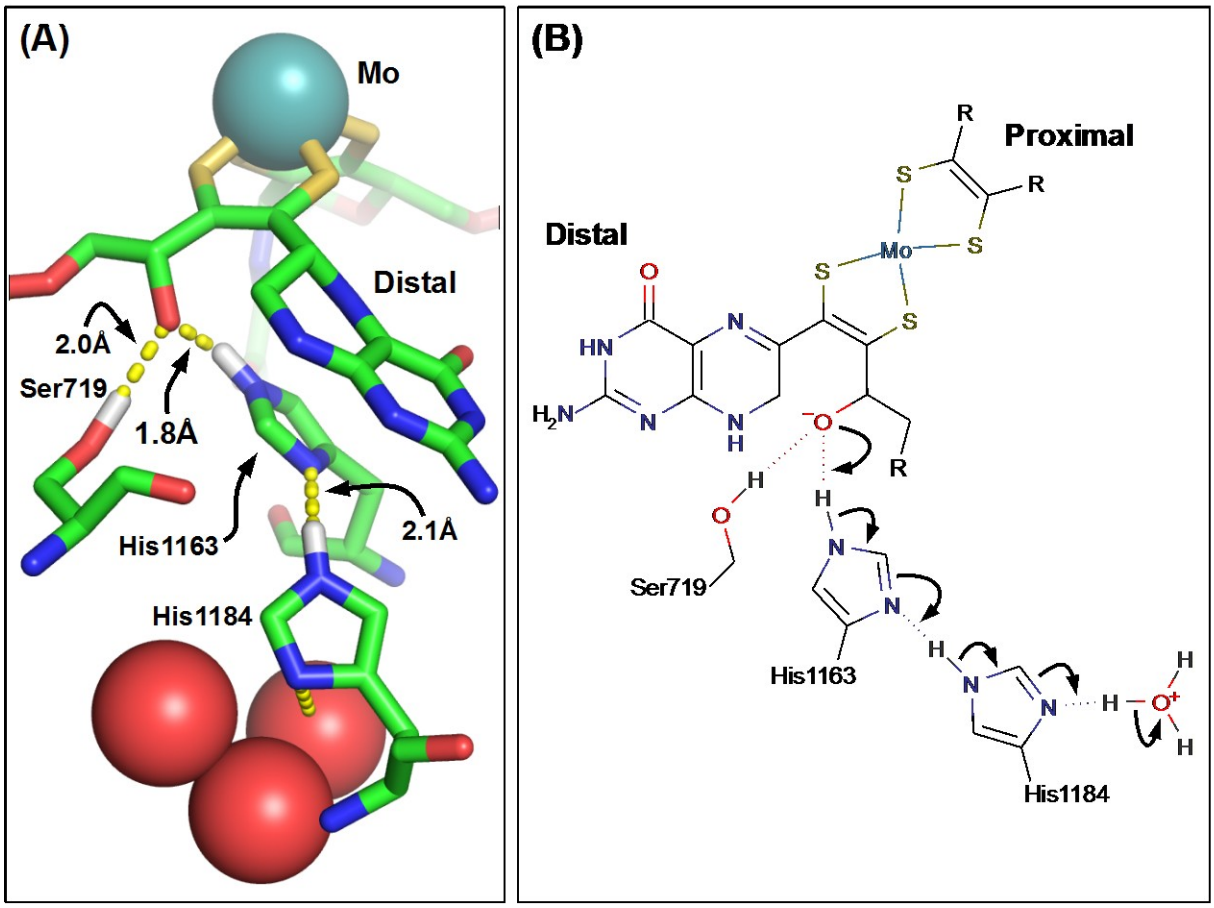

Figure 2.1. Charge transfer relay

(**A**) *Charge-transfer relay in NarG.* Three water molecules are conserved across a range of NarGHI structures, including those described by PDB codes 1Q16, 1R27, 1YZ4 and 1Y5I (Bertero et al. 2003; Jormakka et al. 2004; Bertero et al. 2005). These waters are linked to the pyran oxygen of the bicyclic distal pyranopterin by NarG-His1184 and NarG-H1163. The OG oxygen of NarG-Ser719 is also within H-bonding distance of the pyran oxygen. The image was generated using the Pymol molecular visualization package (version 1.4.1, Schrödinger LLC). (**B**) *Mechanism of charge-transfer between the pyran oxygen and the conserved water molecules*. The indicated charge-transfer results in protonation of the alkoxide anion form of the pyran oxygen. The image was generated using the MarvinSketch software package (www.chemaxon.com). In both panels, some predicted hydrogens have been added for clarity.

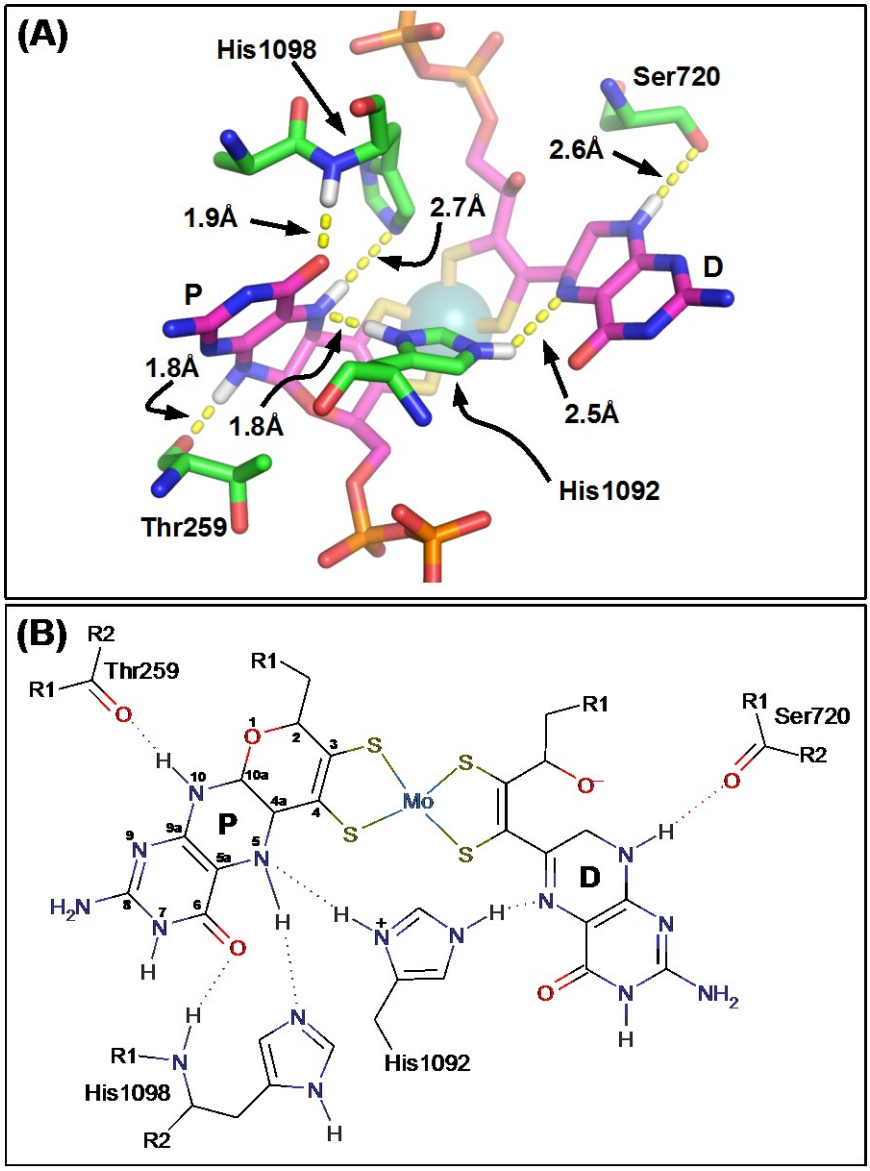

Figure 2.2. Residues defining pyranopterin piperazine ring coordination

(A) *Residues defining pyranopterin piperazine ring coordination.* The image was generated using the NarGHI structure described by PDB code 1Q16 (Bertero et al. 2003). His1092 functions to bridge the two pyranopterins, with its ND1 nitrogen functioning as an H-bond donor to the proximal piperazine N-5 atom, and its NE2 nitrogen functioning as an H-bond donor to the distal piperazine N-5 atom. Note that His1092 is shown in its protonated form to facilitate H-bond donation to both piperazine N-5 atoms. For further details, see the text. (**B**) *Proposed H-bonding network around the piperazine rings of the two pyranopterins*. The proximal pyranopterin (labeled **P**) is shown in its tetrahydro form, with this redox state stabilized by both the bridging His1092 and the stabilizing His1098, while the piperazine of the distal pyranopterin (labeled **D**) is shown in a form equivalent to the 10,10a-dihydro pyranopterin. In both panels, some predicted hydrogens have been added for clarity. Images were generated as described in the legend to **Figure 2.1**.

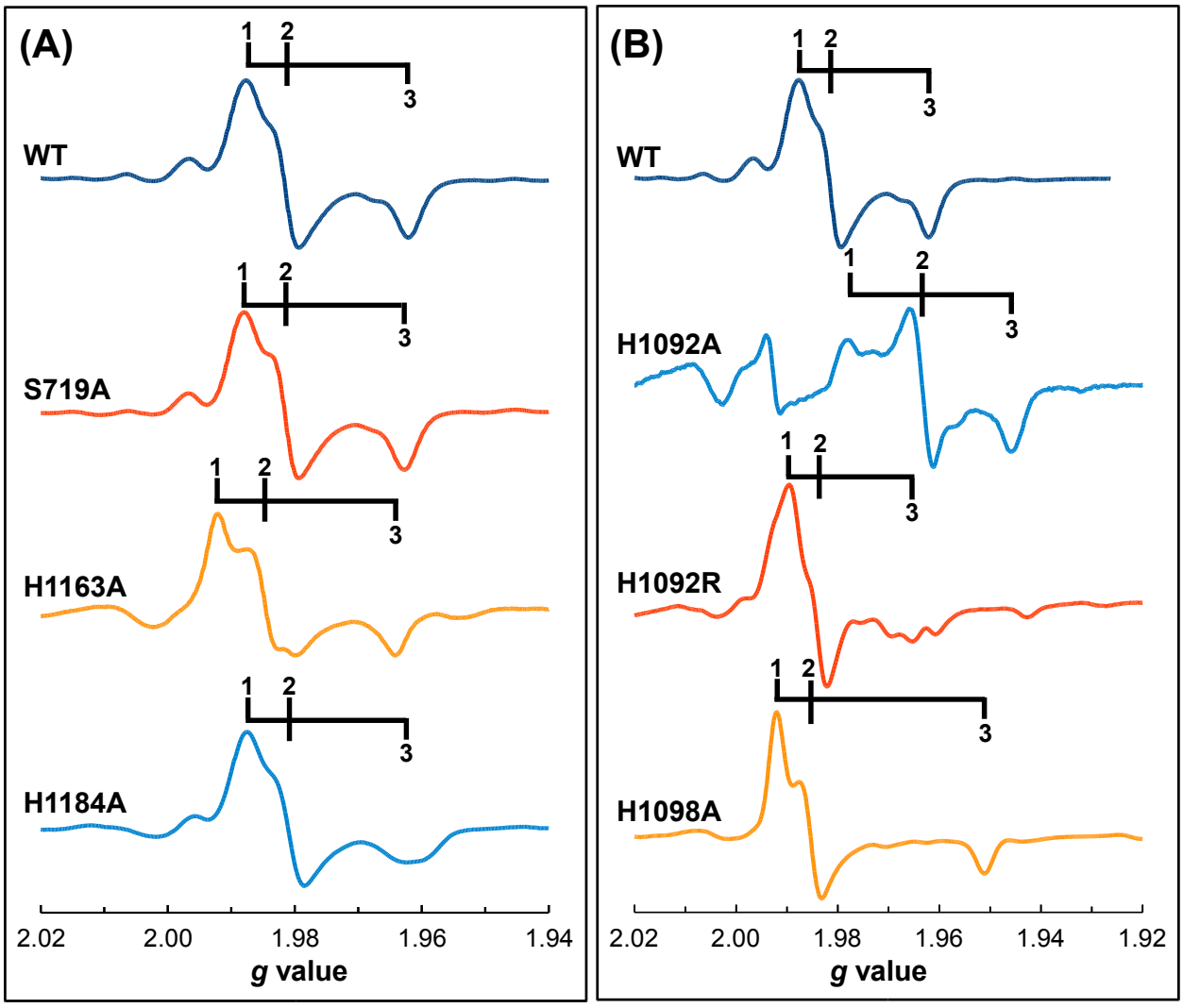

Figure 2.3. Mo(V) EPR spectra of redox-poised NarGHI variants of residues involved in pyranopterin coordination.

(**A**) Ala variants of NarG-Ser719, NarG-His1163 and NarG-H1184; and (**B**) Ala variants of His1092 and His1098, and an Arg variant of His1092. Spectra were recorded at 150K using a microwave power of 20 mW (at a frequency of 9.332 GHz), a modulation amplitude of 4 G_{pp} at a frequency of 100 kHz. Approximate $g_{1,2,3}$ values and potentials at which the samples are poised are: 1.988, 1.982, 1.962 (wild-type, E_h = 150 mV); 1.988, 1.982, 1.962 (Ser719Ala, E_h = 152 mV); 1.992, 1.985, 1.964 (His1163Ala, E_h = 48 mV); 1.986, 1.980, 1.961 (His1184Ala, E_h = 103 mV); 1.978, 1.962, 1.945 (His1092Ala, E_h = -5 mV), 1.989, 1.984, 1.965 (His1092Arg, E_h = 146 mV); 1.992, 1.985, 1.951 (His1098Ala, E_h = 28 mV).

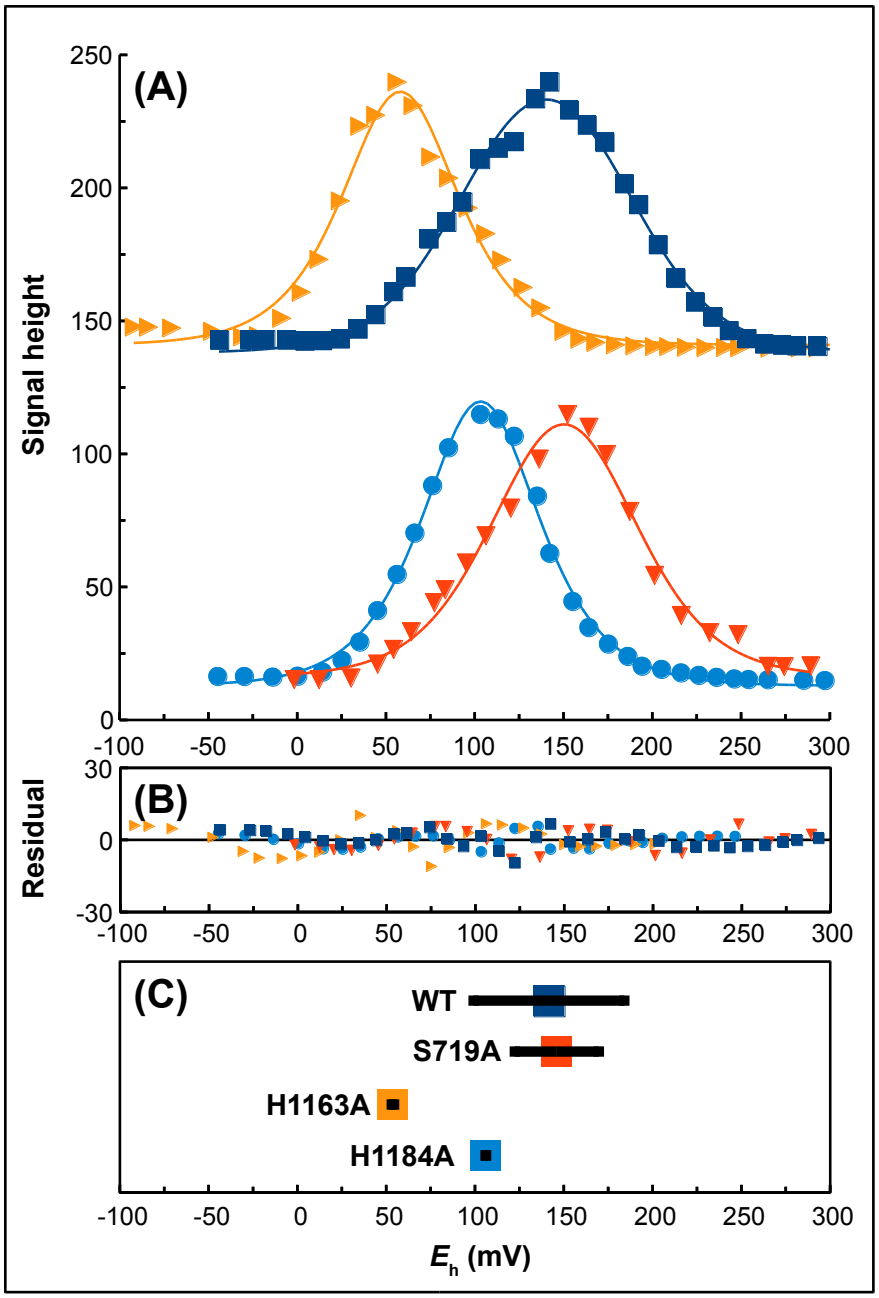

Figure 2.4. Potentiometric titrations of membranes containing variants of residues coordinating the distal pyranopterin of NarGHI

(**A**) Comparison of representative titrations of wild-type (■), Ser719Ala (▼), His1163Ala (►), and His1184Ala (●) enzymes. Data were fit to the following parameters: wild-type, E_m = 140 mV (E_1 = 183 mV, E_2 = 97 mV); Ser719Ala, E_m = 150 mV (E_1 = 176 mV, E_2 = 124 mV); His1163Ala, E_m = 58 mV (E_1 = 49 mV, E_2 = 68 mV); His1184Ala, E_m = 103 mV (E_1 = 96 mV, E_2 = 111 mV). (**B**) Plot of residuals. (**C**) Summary of E_m, E_1 and E_2 values for the variants based on the data presented in Table 1. Colored squares indicate the mean E_m values and the horizontal lines indicate the E_1 and E_2 values in the cases where $E_1 - E_2 > 0$ ($K_{stab} \geq 1$).

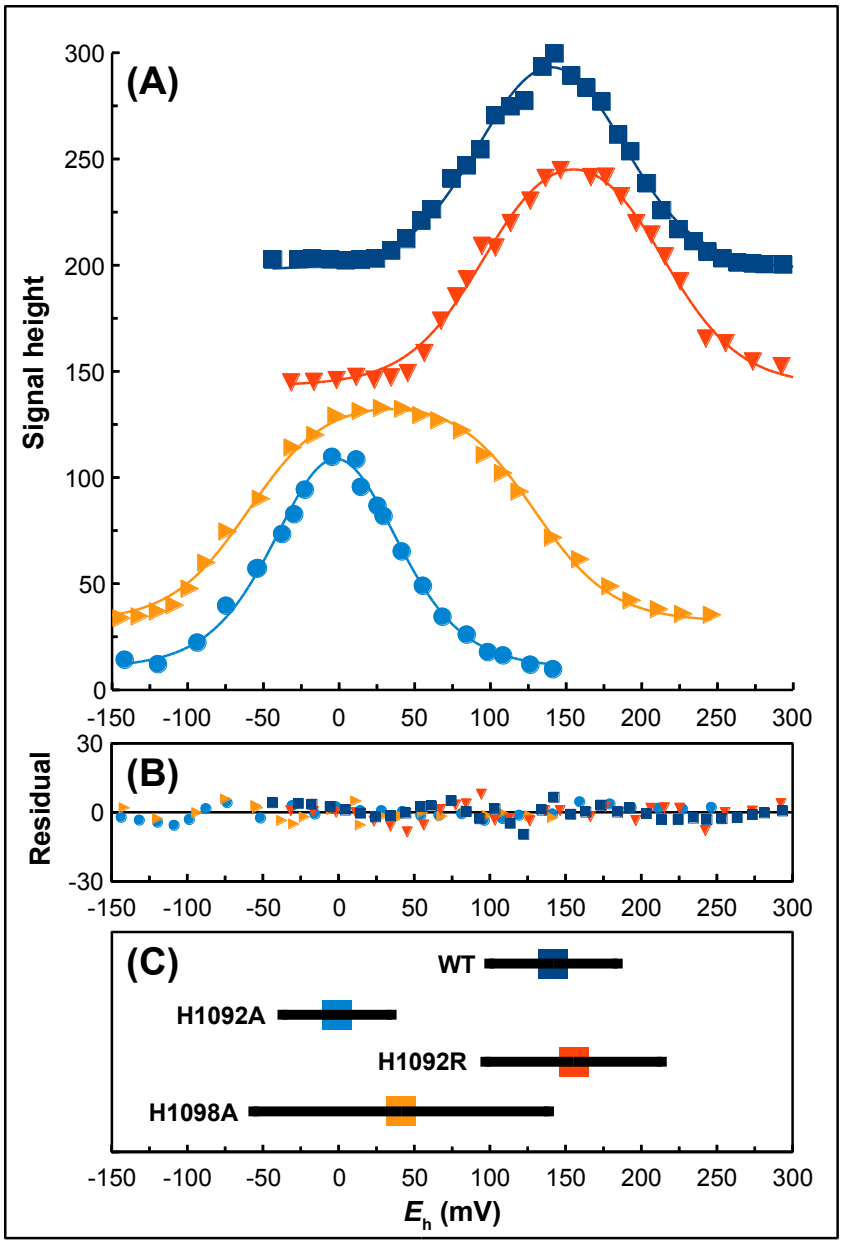

Figure 2.5. Potentiometric titrations of membranes containing variants of His1092 and His1098

(**A**) Comparison of representative titrations of wild-type (■), His1092Arg (▼), His1098Ala (►), and His1092Ala (●) enzymes. Data were fit to the following parameters: wild-type, E_m = 140 mV (E_1 = 183 mV, E_2 = 97 mV); His1092Arg, E_m = 155 mV (E_1 = 213 mV, E_2 = 97 mV); His1098Ala, E_m = 35 mV (E_1 = 129 mV, E_2 = -60 mV); His1092Ala, E_m = -2 mV (E_1 = 24 mV, E_2 = -29 mV). (**B**) Plot of residuals. (**C**) Summary of E_m, E_1 and E_2 values for the variants based on the data presented in **Table 1**. Colored squares indicate the mean E_m values and the horizontal lines indicate the E_1 and E_2 values.

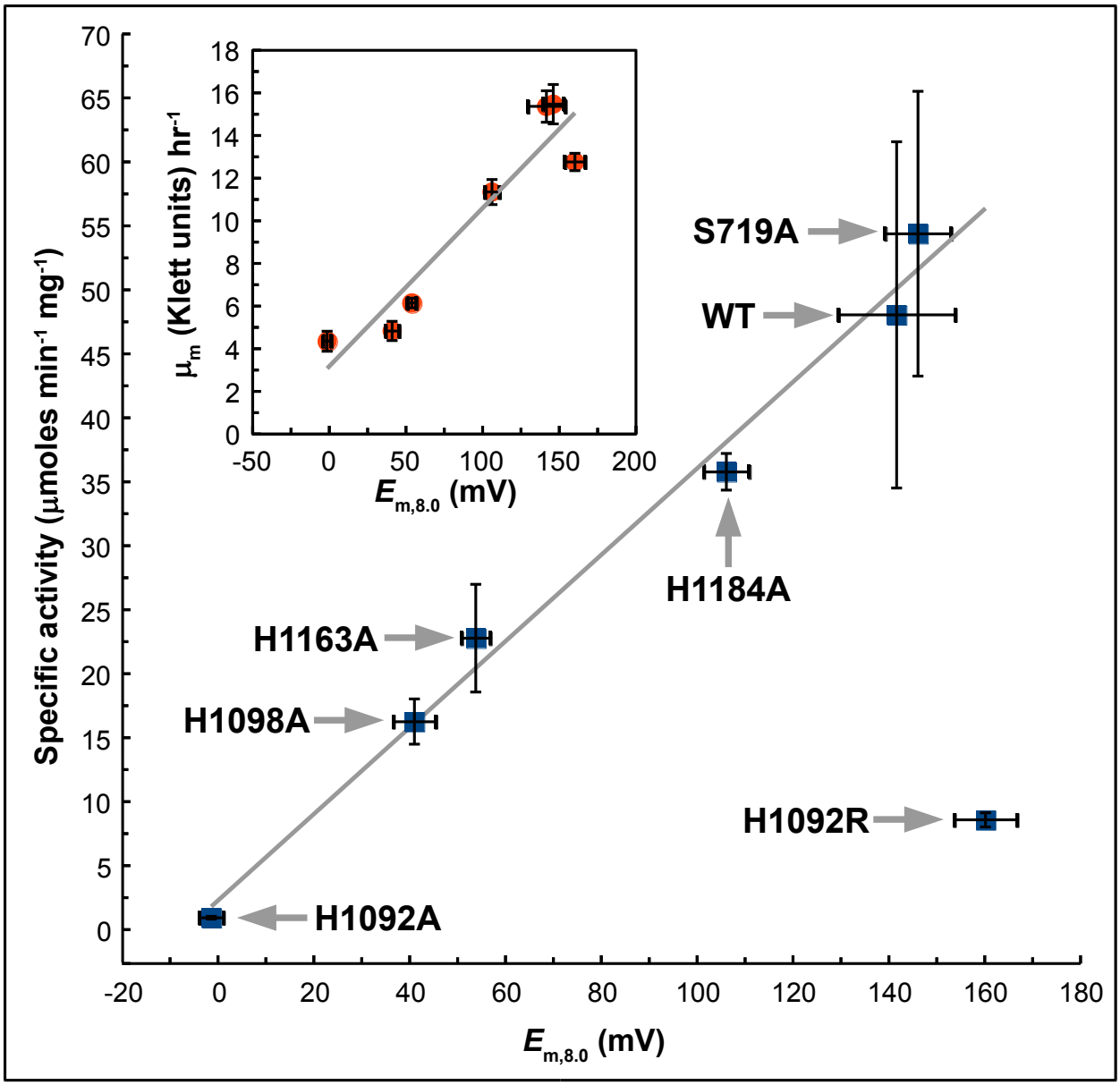

Figure 2.6. Correlation between enzyme activity and overall Mo reduction potential.

Excluding the NarG-His1092Arg variant, a correlation exists between enzyme activity and overall Mo reduction potential (R = 0.99). Inset: Correlation between growth rate and overall Mo reduction potential. Including the NarG-His1092Arg variant, a correlation exists between the maximal rate of respiratory growth on nitrate and overall Mo reduction potential (R = 0.95). Growth rates were calculated using the method of Zwietering et al. (147)

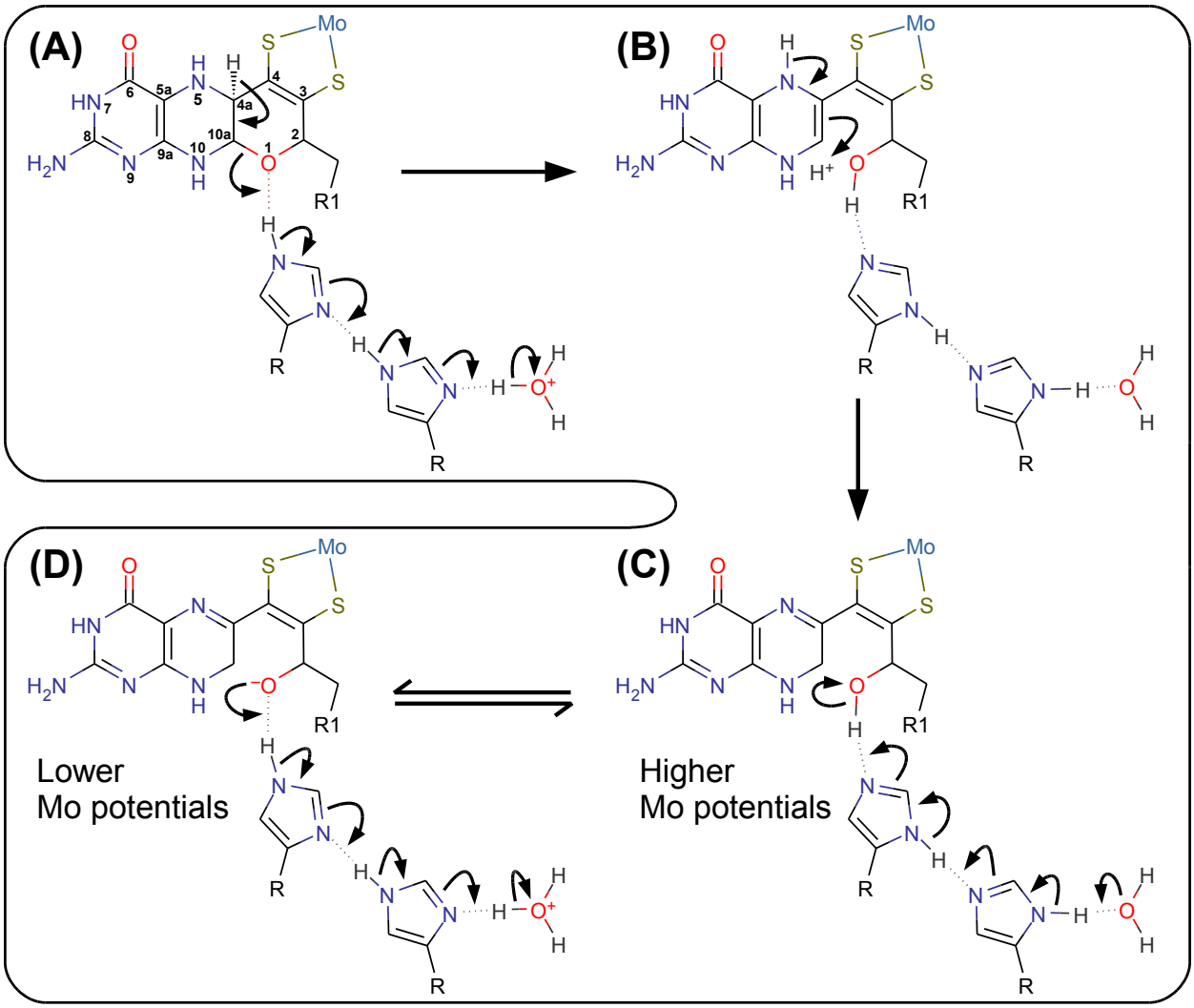

Figure 2.7. Proposed mechanism of pyran ring opening of the distal pyranopterin of NarGHI.

(**A**) The electron transfer relay comprising NarG-His1163 and NarG-His1184 catalyzes proton abstraction from the C-4a atom and pyran ring-opening. The product of this reaction has a piperazine oxidation state and structure equivalent to the 5,10-dihydro pyranopterin (**B**). A tautomerization reaction results in a form equivalent to the 10,10a-dihydro pyranopterin with a protonated oxygen equivalent to O-1. The pterin core of this form is equivalent to the lowest energy dihydropterin tautomer (76, 170). (**C**). The NarG-His1163/His1184 charge-transfer relay functions to modulate an equilibrium between the protonated (hydroxyl) and deprotonated (alkoxide) forms of the bicyclic distal pyranopterin, with the protonated form having a higher overall predicted Mo(VI/VIV) reduction potential than the deprotonated form (**D**).

CHAPTER 3. Conclusions

In Chapter 2, we described how pyranopterin coordination can play a role in guiding electrons and modulating the potential of the Mo. The pyranopterins of the Moco have been undervalued for decades and this work sheds light on them by providing direct experimental evidence showing their functional importance. EPR experiments coupled with redox titrations, along with functional assays, allowed us to accurately assess the changes in Mo electrochemistry and reactivity caused by variants of pyranopterin coordinating residues.

As a part of on-going research of Moco, the Mo active site has always been of focused interest. As mentioned in Section 1.6.6 and illustrated in Figure 1.14, we have a proposal of the reaction mechanism at the active site and the immediate Mo coordination is under investigation, in particular the conserved residues Asn52, His546, and Asn1217. Asn52 is within hydrogen-bonding distance to one of the dithiolene sulfurs and is speculated to have a role in influencing the Mo coordination environment. His546 is within hydrogen-bonding distance to Asp222, the residue that is directly involved in the catalytic mechanism. Asn1217 is within hydrogen-bonding distance to the His546.

The pyranopterin study and the on-going active site study provide an understanding of the Moco. In addition, there are tremendous opportunities to further explore this important cofactor in biology, which is key to understanding the biological diversity of metabolism and evolution of Moco-containing organisms. The current structural and functional information about Moco is only the tip of an iceberg of the knowledge in the field. More effort is required to pursue this curiosity-driven research.

References

1. Hamrick MW (1998) Functional and adaptive significance of primate pads and claws: evidence from new world anthropoids. *Am J Phys Anthropol* 106(2):113–127.

2. Müller DWH, et al. (2013) Assessing the jarman–bell principle: scaling of intake, digestibility, retention time and gut fill with body mass in mammalian herbivores. *Comp Biochem Physiol A Mol Integr Physiol* 164(1):129–140.

3. Price TD (2011) Adaptive radiations: there's something about finches. *Curr Biol* 21(23):R953–R955.

4. Braakman R, Smith E (2014) Metabolic evolution of a deep-branching hyperthermophilic chemoautotrophic bacterium. *PLoS ONE* 9(2). doi:10.1371/journal.pone.0087950.

5. Bryant WA, Faruqi AA, Pinney JW (2013) Analysis of metabolic evolution in bacteria using whole-genome metabolic models. *J Comput Biol* 20(10):755–764.

6. Campbell N, et al. (2008) *Biology* (Pearson, San Francisco). 8th Ed.

7. Mitchell P (1979) Keilin's respiratory chain concept and its chemiosmotic consequences. *Science* 206(4423):1148–1159.

8. Rich P (2003) The molecular machinery of Keilin's respiratory chain. Available at: http://www.biochemsoctrans.org/bst/031/1095/bst0311095.htm [Accessed March 23, 2015].

9. Mitchell P (1967) Proton-translocation phosphorylation in mitochondria, chloroplasts and bacteria: natural fuel cells and solar cells. *Fed Proc* 26:1370–1379.

10. Unden G, Bongaerts J (1997) Alternative respiratory pathways of *Escherichia coli*: energetics and transcriptional regulation in response to electron acceptors. *Biochim Biophys Acta BBA - Bioenerg* 1320(3):217–234.

11. Neidhardt FC, Curtiss R (1996) *Escherichia coli and Salmonella: cellular and molecular biology* (ASM Press).

12. Rolfe MD, et al. (2012) Systems analysis of transcription factor activities in environments with stable and dynamic oxygen concentrations. *Open Biol* 2(7). doi:10.1098/rsob.120091.

13. Gunsalus RP, Park SJ (1994) Aerobic-anaerobic gene regulation in *Escherichia coli*: control by the ArcAB and Fnr regulons. *Res Microbiol* 145(5-6):437–450.

14. Iuchi S, Lin EC (1988) *arcA* (dye), a global regulatory gene in *Escherichia coli* mediating repression of enzymes in aerobic pathways. *Proc Natl Acad Sci U S A* 85(6):1888–1892.

15. Iuchi S, Cameron DC, Lin EC (1989) A second global regulator gene (*arcB*) mediating repression of enzymes in aerobic pathways of *Escherichia coli*. *J Bacteriol* 171(2):868–873.

16. Iuchi S, Matsuda Z, Fujiwara T, Lin EC (1990) The *arcB* gene of *Escherichia coli* encodes a sensor-regulator protein for anaerobic repression of the *arc* modulon. *Mol Microbiol* 4(5):715–727.

17. Iuchi S (1993) Phosphorylation/dephosphorylation of the receiver module at the conserved aspartate residue controls transphosphorylation activity of histidine kinase in sensor protein ArcB of *Escherichia coli*. *J Biol Chem* 268(32):23972–23980.

18. Georgellis D, Lynch AS, Lin EC (1997) *In vitro* phosphorylation study of the Arc two-component signal transduction system of *Escherichia coli*. *J Bacteriol* 179(17):5429–5435.

19. Kwon O, Georgellis D, Lin EC (2000) Phosphorelay as the sole physiological route of signal transmission by the *arc* two-component system of *Escherichia coli*. *J Bacteriol* 182(13):3858–3862.

20. Georgellis D, Kwon O, Lin EC (2001) Quinones as the redox signal for the arc two-component system of bacteria. *Science* 292(5525):2314–2316.

21. Malpica R, Franco B, Rodriguez C, Kwon O, Georgellis D (2004) Identification of a quinone-sensitive redox switch in the ArcB sensor kinase. *Proc Natl Acad Sci U S A* 101(36):13318–13323.

22. Liu X, De Wulf P (2004) Probing the ArcA-P modulon of *Escherichia coli* by whole genome transcriptional analysis and sequence recognition profiling. *J Biol Chem* 279(13):12588–12597.

23. Lynch AS, Lin EC (1996) Transcriptional control mediated by the ArcA two-component response regulator protein of *Escherichia coli*: characterization of DNA binding at target promoters. *J Bacteriol* 178(21):6238–6249.

24. Kang Y, Weber KD, Qiu Y, Kiley PJ, Blattner FR (2005) Genome-wide expression analysis indicates that FNR of *Escherichia coli* K-12 regulates a large number of genes of unknown function. *J Bacteriol* 187(3):1135–1160.

25. Lazazzera BA, Beinert H, Khoroshilova N, Kennedy MC, Kiley PJ (1996) DNA binding and dimerization of the Fe-S-containing FNR protein from *Escherichia coli* are regulated by oxygen. *J Biol Chem* 271(5):2762–2768.

26. Achebach S, Selmer T, Unden G (2005) Properties and significance of apoFNR as a second form of air-inactivated [4Fe-4S]·FNR of *Escherichia coli*. *FEBS J* 272(16):4260–4269.

27. Kiley PJ, Beinert H (1998) Oxygen sensing by the global regulator, FNR: the role of the iron-sulfur cluster. *FEMS Microbiol Rev* 22(5):341–352.

28. Crack J, Green J, Thomson AJ (2004) Mechanism of oxygen sensing by the bacterial transcription factor fumarate-nitrate reduction (FNR). *J Biol Chem* 279(10):9278–9286.

29. Moore LJ, Kiley PJ (2001) Characterization of the dimerization domain in the FNR transcription factor. *J Biol Chem* 276(49):45744–45750.

30. Reinhart F, Achebach S, Koch T, Unden G (2008) Reduced apo-fumarate nitrate reductase regulator (apoFNR) as the major form of FNR in aerobically growing *Escherichia coli*. *J Bacteriol* 190(3):879–886.

31. Khoroshilova N, Popescu C, Münck E, Beinert H, Kiley PJ (1997) Iron-sulfur cluster disassembly in the FNR protein of *Escherichia coli* by O_2: [4Fe-4S] to [2Fe-2S] conversion with loss of biological activity. *Proc Natl Acad Sci U S A* 94(12):6087–6092.

32. Crack JC, et al. (2008) Influence of the environment on the $[4Fe\text{-}4S]^{2+}$ to $[2Fe\text{-}2S]^{2+}$ cluster switch in the transcriptional regulator FNR. *J Am Chem Soc* 130(5):1749–1758.

33. Morpeth FF, Boxer DH (1985) Kinetic analysis of respiratory nitrate reductase from *Escherichia coli* K12. *Biochemistry (Mosc)* 24(1):40–46.

34. Rabin RS, Stewart V (1993) Dual response regulators (NarL and NarP) interact with dual sensors (NarX and NarQ) to control nitrate- and nitrite-regulated gene expression in *Escherichia coli* K-12. *J Bacteriol* 175(11):3259–3268.

35. Cavicchioli R, Chiang RC, Kalman LV, Gunsalus RP (1996) Role of the periplasmic domain of the *Escherichia coli* NarX sensor-transmitter protein in nitrate-dependent signal transduction and gene regulation. *Mol Microbiol* 21(5):901–911.

36. Lee AI, Delgado A, Gunsalus RP (1999) Signal-dependent phosphorylation of the membrane-bound NarX two-component sensor-transmitter protein of *Escherichia coli*: nitrate elicits a superior anion ligand response compared to nitrite. *J Bacteriol* 181(17):5309–5316.

37. Stewart V (1982) Requirement of Fnr and NarL functions for nitrate reductase expression in *Escherichia coli* K-12. *J Bacteriol* 151(3):1320–1325.

38. Iuchi S, Lin EC (1987) The *narL* gene product activates the nitrate reductase operon and represses the fumarate reductase and trimethylamine N-oxide reductase operons in *Escherichia coli*. *Proc Natl Acad Sci U S A* 84(11):3901–3905.

39. Hille R (1996) The Mononuclear Molybdenum Enzymes†. *Chem Rev* 96(7):2757–2816.

40. Schwarz G, Mendel RR, Ribbe MW (2009) Molybdenum cofactors, enzymes and pathways. *Nature* 460(7257):839–847.

41. Romão MJ (2009) Molybdenum and tungsten enzymes: a crystallographic and mechanistic overview. *Dalton Trans* (21):4053–4068.

42. Hille R (2002) Molybdenum and tungsten in biology. *Trends Biochem Sci* 27(7):360–367.

43. Kletzin A, Adams MW (1996) Tungsten in biological systems. *FEMS Microbiol Rev* 18(1):5–63.

44. Rothery RA, Weiner JH (2014) Shifting the metallocentric molybdoenzyme paradigm: the importance of pyranopterin coordination. *J Biol Inorg Chem JBIC Publ Soc Biol Inorg Chem*. doi:10.1007/s00775-014-1194-6.

45. Sigel A, Sigel H, Sigel RKO eds. (2013) *Interrelations between essential metal ions and human diseases* (Springer Netherlands, Dordrecht) Available at: http://link.springer.com/10.1007/978-94-007-7500-8 [Accessed March 31, 2015].

46. Dickinson CJ, Smellie JM (1959) Xanthinuria. *Br Med J* 2(5161):1217–1221.

47. Harkness RA, McCreanor GM, Simpson D, MacFadyen IR (1986) Pregnancy in and incidence of xanthine oxidase deficiency. *J Inherit Metab Dis* 9(4):407–408.

48. Ichida K, et al. (1997) Identification of two mutations in human xanthine dehydrogenase gene responsible for classical type I xanthinuria. *J Clin Invest* 99(10):2391–2397.

49. Garattini E, Mendel R, Romão MJ, Wright R, Terao M (2003) Mammalian molybdo-flavoenzymes, an expanding family of proteins: structure, genetics, regulation, function and pathophysiology. *Biochem J* 372(Pt 1):15–32.

50. Terao M, et al. (2009) Role of the molybdoflavoenzyme aldehyde oxidase homolog 2 in the biosynthesis of retinoic acid: generation and characterization of a knockout mouse. *Mol Cell Biol* 29(2):357–377.

51. Garattini E, Terao M (2013) Aldehyde oxidase and its importance in novel drug discovery: present and future challenges. *Expert Opin Drug Discov* 8(6):641–654.

52. Jordan CG, et al. (1999) Aldehyde oxidase-catalysed oxidation of methotrexate in the liver of guinea-pig, rabbit and man. *J Pharm Pharmacol* 51(4):411–418.

53. Rashidi M-R, Beedham C, Smith JS, Davaran S (2007) *In vitro* study of 6-mercaptopurine oxidation catalysed by aldehyde oxidase and xanthine oxidase. *Drug Metab Pharmacokinet* 22(4):299–306.

54. Rochat B, et al. (1998) Stereoselective biotransformation of the selective serotonin reuptake inhibitor citalopram and its demethylated metabolites by monoamine oxidases in human liver. *Biochem Pharmacol* 56(1):15–23.

55. Schwarz G, Belaidi AA (2013) Molybdenum in human health and disease. *Met Ions Life Sci* 13:415–450.

56. Tan W-H, et al. (2005) Isolated sulfite oxidase deficiency: a case report with a novel mutation and review of the literature. *Pediatrics* 116(3):757–766.

57. Santi C, Bogusz D, Franche C (2013) Biological nitrogen fixation in non-legume plants. *Ann Bot* 111(5):743–767.

58. Mulder EG, Bakema K, Veen WLV (1959) Molybdenum in symbiotic nitrogen fixation and in nitrate assimilation. *Plant Soil* 10(4):319–334.

59. Fan H, Bolhuis H, Stal LJ (2015) Drivers of the dynamics of diazotrophs and denitrifiers in North Sea bottom waters and sediments. *Front Microbiol* 6:738.

60. Bedzyk L, Wang T, Ye RW (1999) The Periplasmic Nitrate Reductase in *Pseudomonas* sp. Strain G-179 Catalyzes the First Step of Denitrification. *J Bacteriol* 181(9):2802–2806.

61. Rajagopalan KV (1991) Novel aspects of the biochemistry of the molybdenum cofactor. *Adv Enzymol Relat Areas Mol Biol* 64:215–290.

62. Rajagopalan KV, Johnson JL (1992) The pterin molybdenum cofactors. *J Biol Chem* 267(15):10199–10202.

63. Mendel RR (2013) The molybdenum cofactor. *J Biol Chem* 288(19):13165–13172.

64. Schwarz G, Mendel RR (2006) Molybdenum cofactor biosynthesis and molybdenum enzymes. *Annu Rev Plant Biol* 57(1):623–647.

65. McWilliams SF, Holland PL (2015) Dinitrogen binding and cleavage by multinuclear iron complexes. *Acc Chem Res* 48(7):2059–2065.

66. Hille R, Hall J, Basu P (2014) The mononuclear molybdenum enzymes. *Chem Rev* 114(7):3963–4038.

67. Leimkühler S, Wuebbens MM, Rajagopalan KV (2011) The history of the discovery of the molybdenum cofactor and novel aspects of its biosynthesis in bacteria. *Coord Chem Rev* 255(9-10):1129–1144.

68. Workun GJ, Moquin K, Rothery RA, Weiner JH (2008) Evolutionary persistence of the molybdopyranopterin-containing sulfite oxidase protein fold. *Microbiol Mol Biol Rev MMBR* 72(2):228–248, table of contents.

69. Rebelo JM, Dias JM, Huber R, Moura JJ, Romão MJ (2001) Structure refinement of the aldehyde oxidoreductase from *Desulfovibrio* gigas (MOP) at 1.28 A. *J Biol Inorg Chem JBIC Publ Soc Biol Inorg Chem* 6(8):791–800.

70. Meyer O, et al. (2000) The role of Se, Mo and Fe in the structure and function of carbon monoxide dehydrogenase. *Biol Chem* 381(9-10):865–876.

71. Dobbek H, Gremer L, Kiefersauer R, Huber R, Meyer O (2002) Catalysis at a dinuclear [CuSMo(==O)OH] cluster in a CO dehydrogenase resolved at 1.1-A resolution. *Proc Natl Acad Sci U S A* 99(25):15971–15976.

72. Mukund S, Adams MW (1990) Characterization of a tungsten-iron-sulfur protein exhibiting novel spectroscopic and redox properties from the hyperthermophilic archaebacterium *Pyrococcus furiosus*. *J Biol Chem* 265(20):11508–11516.

73. Hu Y, Faham S, Roy R, Adams MW, Rees DC (1999) Formaldehyde ferredoxin oxidoreductase from *Pyrococcus furiosus*: the 1.85 A resolution crystal structure and its mechanistic implications. *J Mol Biol* 286(3):899–914.

74. Chan MK, Mukund S, Kletzin A, Adams MW, Rees DC (1995) Structure of a hyperthermophilic tungstopterin enzyme, aldehyde ferredoxin oxidoreductase. *Science* 267(5203):1463–1469.

75. Rothery RA, Workun GJ, Weiner JH (2008) The prokaryotic complex iron–sulfur molybdoenzyme family. *Biochim Biophys Acta BBA - Biomembr* 1778(9):1897–1929.

76. Rothery RA, Stein B, Solomonson M, Kirk ML, Weiner JH (2012) Pyranopterin conformation defines the function of molybdenum and tungsten enzymes. *Proc Natl Acad Sci U S A* 109(37):14773–14778.

77. Kloer DP, Hagel C, Heider J, Schulz GE (2006) Crystal structure of ethylbenzene dehydrogenase from *Aromatoleum aromaticum*. *Structure* 14(9):1377–1388.

78. Bertero MG, et al. (2003) Insights into the respiratory electron transfer pathway from the structure of nitrate reductase A. *Nat Struct Biol* 10(9):681–687.

79. Mendel RR, Hänsch R (2002) Molybdoenzymes and molybdenum cofactor in plants. *J Exp Bot* 53(375):1689–1698.

80. Millar LJ, et al. (2001) Deletion of the *cnxE* gene encoding the gephyrin-like protein involved in the final stages of molybdenum cofactor biosynthesis in *Aspergillus nidulans*. *Mol Genet Genomics MGG* 266(3):445–453.

81. Reiss J, et al. (1998) Mutations in a polycistronic nuclear gene associated with molybdenum cofactor deficiency. *Nat Genet* 20(1):51–53.

82. Stallmeyer B, Drugeon G, Reiss J, Haenni AL, Mendel RR (1999) Human molybdopterin synthase gene: identification of a bicistronic transcript with overlapping reading frames. *Am J Hum Genet* 64(3):698–705.

83. Stallmeyer B, et al. (1999) The neurotransmitter receptor-anchoring protein gephyrin reconstitutes molybdenum cofactor biosynthesis in bacteria, plants, and mammalian cells. *Proc Natl Acad Sci U S A* 96(4):1333–1338.

84. Hänzelmann P, Schindelin H (2006) Binding of 5'-GTP to the C-terminal FeS cluster of the radical S-adenosylmethionine enzyme MoaA provides insights into its mechanism. *Proc Natl Acad Sci U S A* 103(18):6829–6834.

85. Wuebbens MM, Rajagopalan KV (1993) Structural characterization of a molybdopterin precursor. *J Biol Chem* 268(18):13493–13498.

86. Kuper J, Llamas A, Hecht H-J, Mendel RR, Schwarz G (2004) Structure of the molybdopterin-bound Cnx1G domain links molybdenum and copper metabolism. *Nature* 430(7001):803–806.

87. Santamaria-Araujo JA, Wray V, Schwarz G (2012) Structure and stability of the molybdenum cofactor intermediate cyclic pyranopterin monophosphate. *J Biol Inorg Chem JBIC Publ Soc Biol Inorg Chem* 17(1):113–122.

88. Rieder C, et al. (1998) Rearrangement reactions in the biosynthesis of molybdopterin--an NMR study with multiply 13C/15N labelled precursors. *Eur J Biochem FEBS* 255(1):24–36.

89. Hänzelmann P, et al. (2004) Characterization of MOCS1A, an oxygen-sensitive iron-sulfur protein involved in human molybdenum cofactor biosynthesis. *J Biol Chem* 279(33):34721–34732.

90. Mehta AP, Abdelwahed SH, Xu H, Begley TP (2014) Molybdopterin biosynthesis: trapping of intermediates for the MoaA-catalyzed reaction using 2′-deoxyGTP and 2′-chloroGTP as substrate analogues. *J Am Chem Soc* 136(30):10609–10614.

91. Mehta AP, et al. (2013) Catalysis of a new ribose carbon-insertion reaction by the molybdenum cofactor biosynthetic enzyme MoaA. *Biochemistry (Mosc)* 52(7):1134–1136.

92. Hoff T, Schnorr KM, Meyer C, Caboche M (1995) Isolation of two *Arabidopsis* cDNAs involved in early steps of molybdenum cofactor biosynthesis by functional complementation of *Escherichia coli* mutants. *J Biol Chem* 270(11):6100–6107.

93. Hover BM, Tonthat NK, Schumacher MA, Yokoyama K (2015) Mechanism of pyranopterin ring formation in molybdenum cofactor biosynthesis. *Proc Natl Acad Sci* 112(20):6347–6352.

94. Leimkühler S, Freuer A, Araujo JAS, Rajagopalan KV, Mendel RR (2003) Mechanistic studies of human molybdopterin synthase reaction and characterization of mutants identified in group B patients of molybdenum cofactor deficiency. *J Biol Chem* 278(28):26127–26134.

95. Gutzke G, Fischer B, Mendel RR, Schwarz G (2001) Thiocarboxylation of molybdopterin synthase provides evidence for the mechanism of dithiolene formation in metal-binding pterins. *J Biol Chem* 276(39):36268–36274.

96. Rudolph MJ, Wuebbens MM, Rajagopalan KV, Schindelin H (2001) Crystal structure of molybdopterin synthase and its evolutionary relationship to ubiquitin activation. *Nat Struct Biol* 8(1):42–46.

97. Wuebbens MM, Rajagopalan KV (2003) Mechanistic and mutational studies of *Escherichia coli* molybdopterin synthase clarify the final step of molybdopterin biosynthesis. *J Biol Chem* 278(16):14523–14532.

98. Matthies A, Rajagopalan KV, Mendel RR, Leimkühler S (2004) Evidence for the physiological role of a rhodanese-like protein for the biosynthesis of the molybdenum cofactor in humans. *Proc Natl Acad Sci U S A* 101(16):5946–5951.

99. Matthies A, Nimtz M, Leimkühler S (2005) Molybdenum cofactor biosynthesis in humans: identification of a persulfide group in the rhodanese-like domain of MOCS3 by mass spectrometry. *Biochemistry (Mosc)* 44(21):7912–7920.

100. Mendel RR, Schwarz G (2011) Molybdenum cofactor biosynthesis in plants and humans. *Coord Chem Rev* 255(9–10):1145–1158.

101. Schwarz G, et al. (2000) The molybdenum cofactor biosynthetic protein Cnx1 complements molybdate-repairable mutants, transfers molybdenum to the metal binding pterin, and is associated with the cytoskeleton. *Plant Cell Online* 12(12):2455–2471.

102. Llamas A, Otte T, Multhaup G, Mendel RR, Schwarz G (2006) The mechanism of nucleotide-assisted molybdenum insertion into molybdopterin a novel route toward metal cofactor assembly. *J Biol Chem* 281(27):18343–18350.

103. Llamas A, Mendel RR, Schwarz G (2004) Synthesis of adenylated molybdopterin an essential step for molybdenum insertion. *J Biol Chem* 279(53):55241–55246.

104. Blasco F, et al. (2001) The coordination and function of the redox centres of the membrane-bound nitrate reductases. *Cell Mol Life Sci CMLS* 58(2):179–193.

105. Rothery RA, Blasco F, Magalon A, Weiner JH (2001) The diheme cytochrome b subunit (Narl) of *Escherichia coli* nitrate reductase A (NarGHI): structure, function, and interaction with quinols. *J Mol Microbiol Biotechnol* 3(2):273–283.

106. Kalman LV, Gunsalus RP (1989) Identification of a second gene involved in global regulation of fumarate reductase and other nitrate-controlled genes for anaerobic respiration in *Escherichia coli*. *J Bacteriol* 171(7):3810–3816.

107. Goh E-B, et al. (2005) Hierarchical control of anaerobic gene expression in *Escherichia coli* K-12: the nitrate-responsive NarX-NarL regulatory system represses synthesis of the fumarate-responsive DcuS-DcuR regulatory system. *J Bacteriol* 187(14):4890–4899.

108. Zakian S, et al. (2010) Basis of recognition between the NarJ chaperone and the N-terminus of the NarG subunit from *Escherichia coli* nitrate reductase. *FEBS J* 277(8):1886–1895.

109. Blasco F, et al. (1998) NarJ is a specific chaperone required for molybdenum cofactor assembly in nitrate reductase A of *Escherichia coli*. *Mol Microbiol* 28(3):435–447.

110. Volbeda A, et al. (1995) Crystal structure of the nickel-iron hydrogenase from *Desulfovibrio gigas*. *Nature* 373(6515):580–587.

111. Johnson DC, Dean DR, Smith AD, Johnson MK (2005) Structure, function, and formation of biological iron-sulfur clusters. *Annu Rev Biochem* 74(1):247–281.

112. Fritsch J, et al. (2011) The crystal structure of an oxygen-tolerant hydrogenase uncovers a novel iron-sulphur centre. *Nature* 479(7372):249–252.

113. Shomura Y, Yoon K-S, Nishihara H, Higuchi Y (2011) Structural basis for a [4Fe-3S] cluster in the oxygen-tolerant membrane-bound [NiFe]-hydrogenase. *Nature* 479(7372):253–256.

114. Cheng VWT, et al. (2013) A conserved lysine residue controls iron-sulfur cluster redox chemistry in *Escherichia coli* fumarate reductase. *Biochim Biophys Acta* 1827(10):1141–1147.

115. Tang H, Rothery RA, Weiner JH (2013) A variant conferring cofactor-dependent assembly of *Escherichia coli* dimethylsulfoxide reductase. *Biochim Biophys Acta BBA - Bioenerg* 1827(6):730–737.

116. Fedor JG, Rothery RA, Weiner JH (2014) A new paradigm for electron transfer through *Escherichia coli* nitrate reductase A. *Biochemistry (Mosc)* 53(28):4549–4556.

117. Rabenstein D, Greenberg M, Saetre R (1977) Potentiometric and polarimetric studies of complexation of molybdenum(VI) and tungsten(VI) by aspartic-acid and glutamic-acid. *Inorg Chem* 16(5):1241–1243.

118. Iwata M, et al. (2012) The structure of the yeast NADH dehydrogenase (Ndi1) reveals overlapping binding sites for water- and lipid-soluble substrates. *Proc Natl Acad Sci U S A* 109(38):15247–15252.

119. Matz KG, Mtei RP, Leung B, Burgmayer SJN, Kirk ML (2010) Noninnocent Dithiolene Ligands: A New Oxomolybdenum Complex Possessing a Donor−Acceptor Dithiolene Ligand. *J Am Chem Soc* 132(23):7830–7831.

120. Matz KG, Mtei RP, Rothstein R, Kirk ML, Burgmayer SJN (2011) Study of Molybdenum(4+) Quinoxalyldithiolenes as Models for the Noninnocent Pyranopterin in the Molybdenum Cofactor. *Inorg Chem* 50(20):9804–9815.

121. Basu P, Burgmayer SJN (2011) Pterin chemistry and its relationship to the molybdenum cofactor. *Coord Chem Rev* 255(9-10):1016–1038.

122. Sparacino-Watkins C, Stolz JF, Basu P (2014) Nitrate and periplasmic nitrate reductases. *Chem Soc Rev* 43(2):676–706.

123. Grimaldi S, Schoepp-Cothenet B, Ceccaldi P, Guigliarelli B, Magalon A (2013) The prokaryotic Mo/W-bisPGD enzymes family: a catalytic workhorse in bioenergetic. *Biochim Biophys Acta* 1827(8-9):1048–1085.

124. Gonzalez PJ, et al. (2013) Periplasmic nitrate reductases and formate dehydrogenases: Biological control of the chemical properties of Mo and W for fine tuning of reactivity, substrate specificity and metabolic role. *Coord Chem Rev* 257(2):315–331.

125. Moura JJG, Brondino CD, Trincão J, Romão MJ (2004) Mo and W bis-MGD enzymes: nitrate reductases and formate dehydrogenases. *J Biol Inorg Chem JBIC Publ Soc Biol Inorg Chem* 9(7):791–799.

126. Magalon A, Fedor JG, Walburger A, Weiner JH (2011) Molybdenum enzymes in bacteria and their maturation. *Coord Chem Rev* 255(9–10):1159–1178.

127. Mtei RP, et al. (2011) A valence bond description of dizwitterionic dithiolene character in an oxomolybdenum-bis(dithione). *Eur J Inorg Chem* 2011(36):5467–5470.

128. Pushie MJ, George GN (2011) Spectroscopic studies of molybdenum and tungsten enzymes. *Coord Chem Rev* 255(9–10):1055–1084.

129. Jacques JGJ, et al. (2014) Reductive activation in periplasmic nitrate reductase involves chemical modifications of the Mo-cofactor beyond the first coordination sphere of the metal ion. *Biochim Biophys Acta BBA - Bioenerg* 1837(2):277–286.

130. Mtei RP, et al. (2011) Spectroscopic and electronic structure studies of a dimethyl sulfoxide reductase catalytic intermediate: implications for electron- and atom-transfer reactivity. *J Am Chem Soc* 133(25):9762–9774.

131. Baymann F, et al. (2003) The redox protein construction kit: pre-last universal common ancestor evolution of energy-conserving enzymes. *Philos Trans R Soc Lond B Biol Sci* 358(1429):267–274.

132. Schoepp-Cothenet B, et al. (2012) The ineluctable requirement for the trans-iron elements molybdenum and/or tungsten in the origin of life. *Sci Rep* 2:263.

133. Dietrich LEP, Tice MM, Newman DK (2006) The co-evolution of life and Earth. *Curr Biol CB* 16(11):R395–400.

134. Helton ME, et al. (2001) Thermally driven intramolecular charge transfer in an oxo-molybdenum dithiolate complex. *J Am Chem Soc* 123(42):10389–10390.

135. Cerqueira NMFSA, et al. (2009) The effect of the sixth sulfur ligand in the catalytic mechanism of periplasmic nitrate reductase. *J Comput Chem* 30(15):2466–2484.

136. Feng C, Tollin G, Enemark JH (2007) Sulfite oxidizing enzymes. *Biochim Biophys Acta* 1774(5):527–539.

137. Jormakka M, et al. (2008) Molecular mechanism of energy conservation in polysulfide respiration. *Nat Struct Mol Biol* 15(7):730–737.

138. Jormakka M, Törnroth S, Byrne B, Iwata S (2002) Molecular basis of proton motive force generation: structure of formate dehydrogenase-N. *Science* 295(5561):1863–1868.

139. Coelho C, et al. (2011) The crystal structure of *Cupriavidus necator* nitrate reductase in oxidized and partially reduced states. *J Mol Biol* 408(5):932–948.

140. Pascal MC, Burini JF, Ratouchniak J, Chippaux M (1982) Regulation of the nitrate reductase operon: effect of mutations in chlA, B, D and E genes. *Mol Gen Genet MGG* 188(1):103–106.

141. Guigliarelli B, et al. (1996) Complete coordination of the four Fe-S centers of the beta subunit from *Escherichia coli* nitrate reductase. Physiological, biochemical, and EPR characterization of site-directed mutants lacking the highest or lowest potential [4Fe-4S] clusters. *Biochemistry (Mosc)* 35(15):4828–4836.

142. Sambrook J, Russell DW (2001) *Molecular cloning: a laboratory manual* (CSHL Press).

143. Cammack R, Weiner JH (1990) Electron paramagnetic resonance spectroscopic characterization of dimethyl sulfoxide reductase of *Escherichia coli*. *Biochemistry (Mosc)* 29(36):8410–8416.

144. Laemmli UK (1970) Cleavage of Structural Proteins during the Assembly of the Head of Bacteriophage T4. *Nature* 227(5259):680–685.

145. Rothery RA, Weiner JH (1991) Alteration of the iron-sulfur cluster composition of *Escherichia coli* dimethyl sulfoxide reductase by site-directed mutagenesis. *Biochemistry (Mosc)* 30(34):8296–8305.

146. Rothery RA, Grant JL, Johnson JL, Rajagopalan KV, Weiner JH (1995) Association of molybdopterin guanine dinucleotide with *Escherichia coli* dimethyl sulfoxide reductase: effect of tungstate and a *mob* mutation. *J Bacteriol* 177(8):2057–2063.

147. Zwietering MH, Jongenburger I, Rombouts FM, van 't Riet K (1990) Modeling of the bacterial growth curve. *Appl Environ Microbiol* 56(6):1875–1881.

148. Johnson JL, Rajagopalan KV (1982) Structural and metabolic relationship between the molybdenum cofactor and urothione. *Proc Natl Acad Sci U S A* 79(22):6856–6860.

149. Johnson JL, Indermaur LW, Rajagopalan KV (1991) Molybdenum cofactor biosynthesis in *Escherichia coli*. Requirement of the *chlB* gene product for the formation of molybdopterin guanine dinucleotide. *J Biol Chem* 266(19):12140–12145.

150. Rothery RA, et al. (1998) The molybdenum cofactor of *Escherichia coli* nitrate reductase A (NarGHI). Effect of a *mobAB* mutation and interactions with [Fe-S] clusters. *J Biol Chem* 273(13):7462–7469.

151. Rothery RA, Trieber CA, Weiner JH (1999) Interactions between the molybdenum cofactor and iron-sulfur clusters of *Escherichia coli* dimethylsulfoxide reductase. *J Biol Chem* 274(19):13002–13009.

152. Hastings SF, et al. (1998) Identification of a stable semiquinone intermediate in the purified and membrane bound ubiquinol oxidase-cytochrome bd from *Escherichia coli*. *Eur J Biochem FEBS* 255(1):317–323.

153. Ohnishi T, et al. (1981) Thermodynamic and electron paramagnetic resonance characterization of flavin in succinate dehydrogenase. *J Biol Chem* 256(11):5577–5582.

154. Lowry OH, Rosebrough NJ, Farr AL, Randall RJ (1951) Protein Measurement with the Folin Phenol Reagent. *J Biol Chem* 193(1):265–275.

155. Markwell MA, Haas SM, Bieber LL, Tolbert NE (1978) A modification of the Lowry procedure to simplify protein determination in membrane and lipoprotein samples. *Anal Biochem* 87(1):206–210.

156. Elliott SJ, et al. (2003) Voltammetric studies of the catalytic mechanism of the respiratory nitrate reductase from *Escherichia coli*: how nitrate reduction and inhibition depend on the oxidation state of the active site. *Biochemistry (Mosc)* 43(3):799–807.

157. Vincent SP, Bray RC (1978) Electron-paramagnetic-resonance studies on nitrate reductase from *Escherichia coli* K12. *Biochem J* 171(3):639–647.

158. George GN, Bray RC, Morpeth FF, Boxer DH (1985) Complexes with halide and other anions of the molybdenum centre of nitrate reductase from *Escherichia coli*. *Biochem J* 227(3):925–931.

159. George GN, et al. (1989) X-ray-absorption and electron-paramagnetic-resonance spectroscopic studies of the environment of molybdenum in high-pH and low-pH forms of *Escherichia coli* nitrate reductase. *Biochem J* 259(3):693–700.

160. Guigliarelli B, et al. (1992) EPR and redox characterization of iron-sulfur centers in nitrate reductases A and Z from *Escherichia coli*. Evidence for a high-potential and a low-potential class and their relevance in the electron-transfer mechanism. *Eur J Biochem FEBS* 207(1):61–68.

161. Rothery RA, et al. (2004) The catalytic subunit of *Escherichia coli* nitrate reductase A contains a novel [4Fe-4S] cluster with a high-spin ground state. *Biochemistry (Mosc)* 43(18):5324–5333.

162. Vincent SP (1979) Oxidation--reduction potentials of molybdenum and iron--sulphur centres in nitrate reductase from *Escherichia coli*. *Biochem J* 177(2):757–759.

163. Frangioni B, et al. (2004) In *Rhodobacter sphaeroides* respiratory nitrate reductase, the kinetics of substrate binding favors intramolecular electron transfer. *J Am Chem Soc* 126(5):1328–1329.

164. Heffron K, Léger C, Rothery RA, Weiner JH, Armstrong FA (2001) Determination of an optimal potential window for catalysis by *E. coli* dimethyl sulfoxide reductase and hypothesis on the role of Mo(V) in the reaction pathway. *Biochemistry (Mosc)* 40(10):3117–3126.

165. Wardman P (1991) The reduction potential of benzyl viologen: an important reference compound for oxidant/radical redox couples. *Free Radic Res Commun* 14(1):57–67.

166. Wallace BJ, Young IG (1977) Role of quinones in electron transport to oxygen and nitrate in *Escherichia coli*. Studies with a *ubiA- menA-* double quinone mutant. *Biochim Biophys Acta* 461(1):84–100.

167. Lanciano P, Vergnes A, Grimaldi S, Guigliarelli B, Magalon A (2007) Biogenesis of a respiratory complex is orchestrated by a single accessory protein. *J Biol Chem* 282(24):17468–17474.

168. Chan CS, Howell JM, Workentine ML, Turner RJ (2006) Twin-arginine translocase may have a role in the chaperone function of NarJ from *Escherichia coli*. *Biochem Biophys Res Commun* 343(1):244–251.

169. Rothery RA, et al. (2010) Protein crystallography reveals a role for the FS0 cluster of *Escherichia coli* nitrate reductase A (NarGHI) in enzyme maturation. *J Biol Chem* 285(12):8801–8807.

170. Greatbanks SP, Hillier IH, Garner CD, Joule JA (1997) The relative stabilities of dihydropterins; a comment on the structureof Moco, the cofactor of the oxomolybdoenzymes. *J Chem Soc Perkin Trans 2* (8):1529–1534.